

# A physical approach for a simultaneous retrieval of sounding, surface, hydrometeor, and cryospheric parameters from SNPP/ATMS

S.-A. Boukabara,<sup>1</sup> K. Garrett,<sup>2</sup> C. Grassotti,<sup>3</sup> F. Iturbide-Sanchez,<sup>4</sup> W. Chen,<sup>2</sup> Z. Jiang,<sup>3</sup> S. A. Clough,<sup>3</sup> X. Zhan,<sup>1</sup> P. Liang,<sup>3</sup> Q. Liu,<sup>5</sup> T. Islam,<sup>6</sup> V. Zubko,<sup>3</sup> and A. Mims<sup>3</sup>

Received 9 July 2013; revised 24 September 2013; accepted 20 October 2013; published 19 November 2013.

[1] We present in this study the results obtained when applying a physical algorithm based on a variational methodology to data from the Advanced Technology Microwave Sounder (ATMS) onboard the Suomi National Polar-Orbiting Partnership (SNPP) for a consistent retrieval of geophysical data in all weather conditions. The algorithm, which runs operationally at the U.S. National Oceanic and Atmospheric Administration, is applied routinely to a number of sounders from the Polar-Orbiting Operational Environmental Satellites, the Defense Meteorological Satellite Program, and the European Meteorological Operational satellite constellations. The one-dimension variational (1DVAR) methodology, which relies on a forward operator, the Community Radiative Transfer Model, allows for solving the inversion of the radiometric measurements into geophysical parameters which have a direct impact on the brightness temperatures. The parameters that are produced by this Microwave Integrated Retrieval System algorithm include the atmospheric temperature  $T(p)$ , moisture  $Q(p)$ , and vertically integrated total precipitable water; and the surface skin temperature and emissivity as well as the hydrometeor products of nonprecipitating cloud liquid water and rain- and ice-water paths. In this algorithm, a simple postprocessing is applied to the 1DVAR-generated emissivity to derive cryospheric products (snow water equivalent and sea-ice concentration) when the data are measured over these surfaces. The postprocessing is also applied to the hydrometeors products to generate a surface rainfall rate. This comprehensive set of sounding, surface, hydrometeor, and cryospheric products generated from SNPP/ATMS is therefore radiometrically consistent, meaning that when input to the forward operator, it will allow the simulation of the actual brightness temperatures measurements within noise levels. The geophysical consistency between the products, also critical, is satisfied due to the physical approach adopted and the geophysical constraints introduced through the correlation matrix used in the variational system. The results shown in this paper confirm that the performances of all products are within the expected accuracy and precision figures and comparable to performances usually obtained with single-parameter-dedicated algorithms, with the added value that the inverted products are both radiometrically and geophysically consistent.

**Citation:** Boukabara, S.-A., et al. (2013), A physical approach for a simultaneous retrieval of sounding, surface, hydrometeor, and cryospheric parameters from SNPP/ATMS, *J. Geophys. Res. Atmos.*, 118, 12,600–12,619, doi:10.1002/2013JD020448.

## 1. Introduction

[2] The study seeks to assess the Suomi National Polar-orbiting Partnership (SNPP)/Advanced Technology Microwave Sounder (ATMS)-derived products performances when

using a physical algorithm. This is done through a number of intercomparisons with several references. The algorithm itself is already operational for a number of sensors, mainly microwave sounders, onboard the Polar-orbiting Operational Environmental Satellites (POES) (NOAA 18 and 19), MetOp (A and B), and DMSP (F16 and F18) constellations. The algorithm has also been applied in research mode for the Tropical Rainfall Measuring Mission Microwave Imager and to the French-Indian Megha-Tropiques' Microwave Analysis and Detection of Rain and Atmospheric Structures and Sounder for Probing Vertical Profiles of Humidity sensors as well as the recently launched Global Change Observation Mission-Water Advanced Microwave Scanning Radiometer (AMSR-2) sensor. When expanded to SNPP/ATMS, it was configured to run at the highest ATMS spatial resolution

<sup>1</sup>NOAA/NESDIS/STAR, College Park, Maryland, USA.

<sup>2</sup>RTI, College Park, MD, USA.

<sup>3</sup>AER Inc, College Park, MD, USA.

<sup>4</sup>IMSG Inc., College Park, MD.

<sup>5</sup>University of maryland, College Park, MD, USA.

<sup>6</sup>Colorado State University.

Corresponding author: S.-A. Boukabara, NOAA/NESDIS/ORA, College Park, MD 20740, USA. (Sid.Boukabara@noaa.gov)

©2013. American Geophysical Union. All Rights Reserved.  
2169-897X/15/10.1002/2013JD020448

possible. Section 2 describes in more detail the main components and the mathematical basis of the algorithm itself. This is followed by a description of the SNPP/ATMS data and their radiometric quality (section 3). The physical algorithm used aims at inverting all the geophysical parameters in a consistent fashion (both radiometrically and geophysically). Section 4 focuses on system implementation and the performance verification methodology. The final sections (5, 6, 7, and 8) concentrate on presenting the performance of the atmospheric, surface, hydrometeors, and cryospheric products, respectively.

## 2. Description of the Algorithm

[3] The Microwave Integrated Retrieval System (MiRS) algorithm used in this study is a one-dimensional variational inversion scheme (1DVAR) that employs the Community Radiative Transfer Model (CRTM) as the forward and adjoint operator [Liu *et al.*, 2012] and aims at minimizing a cost function similar to the Numerical Weather Prediction (NWP) variational assimilation. It is described in detail in Boukabara *et al.* [2010, 2011]; Kongoli *et al.* [2011], and Iturbide-Sánchez *et al.* [2011], but for the sake of completeness, the most important characteristics of the algorithm are recalled here. The most important characteristic relates to solving simultaneously for the surface and the atmospheric parameters including hydrometeors, making it an algorithm valid in all weather conditions, as long as the CRTM is valid in those conditions. It is important to add the caveat that the parameters that the algorithm effectively inverts under the different meteorological conditions differ and depend on the geophysical situation and the existence of a radiometric signal. The surface parameters for example (as well as atmospheric moisture) do not have a significant impact on the measurements in heavily precipitating conditions, making their retrieval not possible. From a physical point of view, when the radiometric signal is saturated in these conditions, the Jacobians with respect to surface parameters are null for these surface parameters, which means that the state vector does not move from the mean background values. So even if technically the inversion is producing a surface parameter, this is entirely based on the background information, not on actual radiometric signal. The MiRS algorithm outputs contain information that allows the user to distinguish radiometric-based retrievals from those that rely on background.

[4] The usage of the CRTM simplifies the extension of the algorithm to new sensors, since all the specificities of the sensor are incorporated within the CRTM, which enables the MiRS generic handling of the brightness temperatures simulation and Jacobians. For this reason, the extension of MiRS to SNPP/ATMS was technically achieved in approximately 3 months, which allowed us to focus more intensively on Cal/Val science issues rather than on software implementation issues. The validation of the derived products is the subject of this study. The surface is represented in MiRS by its temperature and its emissivity spectrum, therefore fully accounting for the surface boundary conditions and making the algorithm applicable over all surfaces. The only difference between the retrievals over the different surfaces is the spectral shape and the amplitude of the emissivity spectrum

inverted. Because the state vector is inverted in one single block, the geophysical background covariance matrix in MiRS plays a critical role. This matrix represents the natural correlations between all parameters including atmospheric temperature and moisture, skin temperature, and the hydrometeors and cloud parameters. It is derived carefully using a combination of NWP model runs and climatological data sets. When the retrieval is initiated, one of the first steps (after bias removal) is to preclassify the surface scene corresponding to the measurements in order to select the proper surface emissivity background covariance. The surface types considered are (1) ocean, (2) land, (3) snow, and (4) sea ice. Precomputed emissivity background means and covariance matrices are loaded upfront, and the appropriate one is selected on a measurement by measurement basis. The preclassification algorithm is generated offline based on a regression between collocated measurements and computed emissivities. Over ocean, these emissivities are computed using a physical model, and over non-ocean surfaces, these are generated analytically using Prigent *et al.* [2008]. More details on the preclassification and the emissivity handling are described in detail in Boukabara *et al.* [2011]. It is worth noting that the actual retrieval is performed in a reduced space using an Empirical Orthogonal Functions projection, therefore ensuring a stable and fast inversion using small matrices but also forfeiting any prospect of inverting small-scale vertical structure information. The potential loss of information content due to the reduced space inversion is likely to be minor since the vertical weighting functions of the 22 ATMS sounding channels are rather smooth (see Figure 1). After the 1DVAR process is applied, other products are derived either by performing simple vertical integration (the case of the total precipitable water (TPW), cloud liquid water (CLW), ice-water path (IWP), and rain water path (RWP)) or by performing a more elaborate postprocessing (the case of rainfall rate and cryospheric products).

## 3. Description of SNPP/ATMS

[5] The Suomi National Polar-orbiting Partnership (SNPP) launched in 2011 is the first of a series of next-generation U.S. polar-orbiting satellites. SNPP contains the same main instruments that will be carried on the Joint Polar Satellite System 1, which is scheduled to launch in early 2017. One of the main advantages of the ATMS sensor with respect to its predecessors Advanced Microwave Sounding Unit (AMSU) and Microwave Humidity Sounder (MHS) is the wider swath that practically eliminates the orbital gaps as can be seen in some of the maps shown in this paper. The calibration and instrument characteristics of the sensor have been presented; see for example, Zou *et al.* [2013]. As mentioned earlier, the data from SNPP/ATMS are preprocessed in the MiRS algorithm in order to remove radiometric biases and/or radiative transfer modeling errors between the measurements and the forward operator CRTM. As part of this preprocessing, the noise level specific to each orbit (for each sensor channel) is also computed and input to the 1DVAR algorithm, which needs this information for the proper weighing to be applied to the radiances. In addition to the noise computation and the bias removal, the ATMS brightness temperatures for all channels are footprint matched

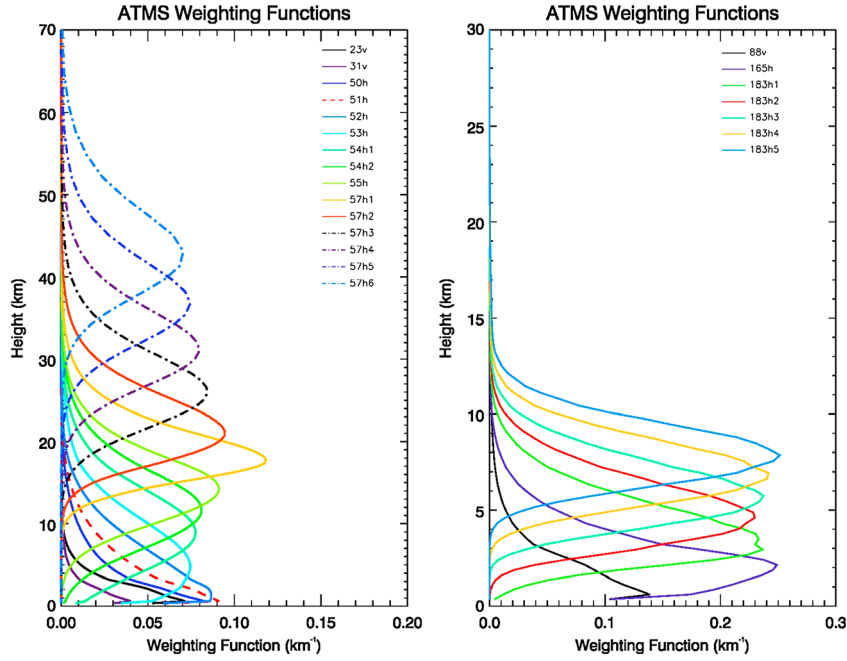


**Figure 1.** Temperature weighting functions for ATMS channels (left) 1–15 and (right) 16–22.

in MiRS using a Backus Gilbert approach developed by the UK Meteorological Office [Atkinson, 2011]. In this phase, spatial averaging of ATMS footprints is performed with the Advanced TIROS Operational Vertical Sounder and Advanced Very High Resolution Radiometer Preprocessing Package developed at the European Organisation for the Exploitation of Meteorological Satellites Satellite Application Facility on Numerical Weather Prediction. The spatial averaging is only performed for ATMS channels 1 and 2, where a Fourier transform is applied to a field of brightness temperatures to increase the resolution from  $5.2^\circ$  beam width to  $3.3^\circ$ . It is known that satellite spatial resolution enhancement techniques tend to increase the noise level of the resulting data [Long and Daum, 1998]. Generally, the higher the sampling of the original data, the better the resolution enhancement result could be. In this exercise, care was given to ensure that the resulting noise amplification was not excessive and remained below the Radiative Transfer Model (RTM) uncertainty levels.

#### 4. Ensuring Radiometric and Geophysical Consistency

[6] A necessary condition to meet in the MiRS 1DVAR, to ensure radiometric consistency, is that the retrieved geophysical parameters are consistent with the brightness temperatures observed by SNPP. For the retrieved scene to meet the convergence criteria, simulated brightness temperatures using the retrieved geophysical parameters as inputs and CRTM as the forward operator must fit the observed brightness temperatures within the instrument noise levels and specified uncertainty of the radiative transfer model. The convergence is defined by the chi-square metric computed by the nonconstrained cost function [Boukabara, 2011]. Convergence is strictly defined by  $\varphi^2$  values less than 1, although values less than 5 are deemed acceptable. In clear-

sky or cloudy conditions, the information content contained within the ATMS observations relates to emission signal from both the surface and atmosphere. The surface emission component is dependent upon the underlying surface type and properties such as moisture content and temperature, while the atmospheric component is dependent upon the profiles of temperature, water vapor, and cloud. Figure 1 shows the temperature weighting functions for all ATMS channels for a standard tropical atmosphere.

[7] In the MiRS 1DVAR, the assumption for the first retrieval attempt is exactly this scenario: that the observed signal is solely that of atmospheric and/or surface emission and that there is no scattering signal from rain or ice hydrometeors. When the convergence is assessed globally, as in Figure 2 (left), many nonconvergent retrievals are illustrated by  $\varphi^2$  values greater than 5 (roughly 5% of the observations).

[8] Qualitatively, most of these nonconvergent retrievals are found to be associated with precipitation which is not accounted for in the first-attempt retrieval state vector. In practice, MiRS performs a second attempt on all nonconvergent retrievals, but instead of accounting for only surface or atmospheric emission, rain and graupel hydrometeors are included in the retrieved state vector to account for atmospheric scattering in the observed brightness temperatures. The effect on nonconvergence can be seen in Figure 2 (right), where almost 100% of the retrievals have  $\varphi^2$  values below 5, although handling of surface conditions can also influence convergence as is seen over Antarctica. Essentially, the convergence as defined (and achieved) above ensures the radiometric consistency of the retrievals.

[9] In addition to the radiometric consistency, which is a necessary but not sufficient condition for any retrieval, geophysical parameters must be properly constrained and physically consistent with each other. Many constraints are implemented in MiRS to ensure this aspect. The computation of the derivatives and the simulations of the measurements

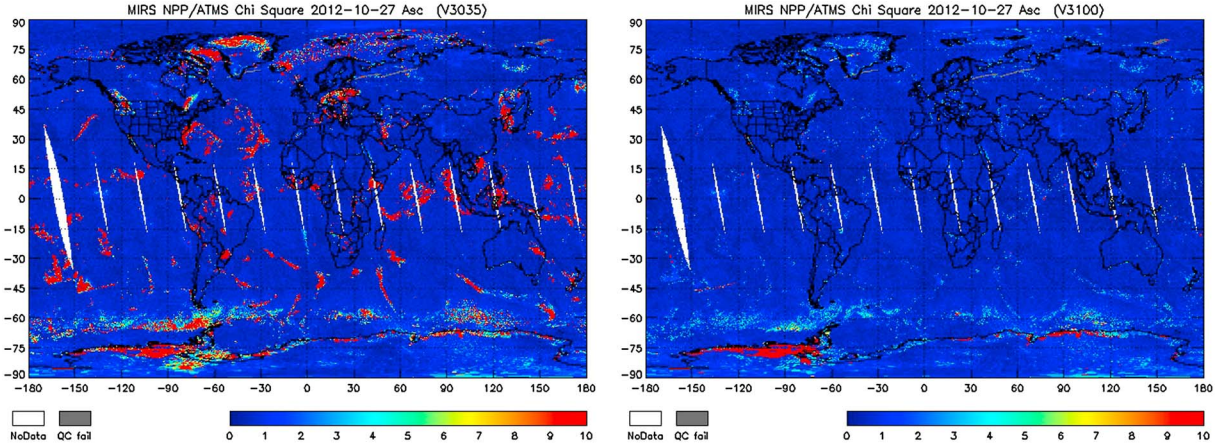


**Figure 2.** Chi-square for MiRS SNPP/ATMS retrieval for case day 27 October 2012 (left) after first attempt retrieval where hydrometeors retrieval is turned off and (right) when a second attempt is performed with scattering turned on.

are both based on a physical model (CRTM) which provides, on an iteration by iteration basis, a strong physical constraint on how the inverted parameters are adjusted during the retrieval process. Another significant constraint, perhaps the most important one, is based on the a priori information used for both the surface and the atmospheric parameters. The emissivity covariance matrix and background emissivity spectra are generated for different surface types. Figure 3 shows the background emissivity spectra for ocean, sea ice, land, and snow surface types, along with their variance. Note that polarizations are not identical for all channels. At this time, all angles are represented in the mean and covariance matrices. A future improvement might be the stratification of these by viewing angle. It is therefore important that the variance is adequate to allow emissivity departures from the background values if the signal from surface-sensitive channels (determined from CRTM jacobians) exists. This will help in the handling of off-average observing angles

but also of extreme situations. For example, heavy rainfall events and the resulting added soil moisture to land surface dramatically affects the magnitude and shape of the land emissivity spectrum. The loose constraint in the background covariance will allow accommodating this situation and will permit the algorithm to converge toward the solution.

[10] The atmospheric constraints are equally important. The correlation between temperature, water vapor, clouds, and precipitation, along with correlation with the surface skin temperature, must ensure physical consistency between the retrieved state vector parameters. The correlations and cross correlations for retrieved geophysical parameters are illustrated in Figure 4.

[11] The covariances used in MiRS ensure that the geophysical state vector variables are coherently retrieved and that the retrieval takes advantage of known natural correlations between these variables. It is important to note that no information from forecast runs is used in any of the MiRS

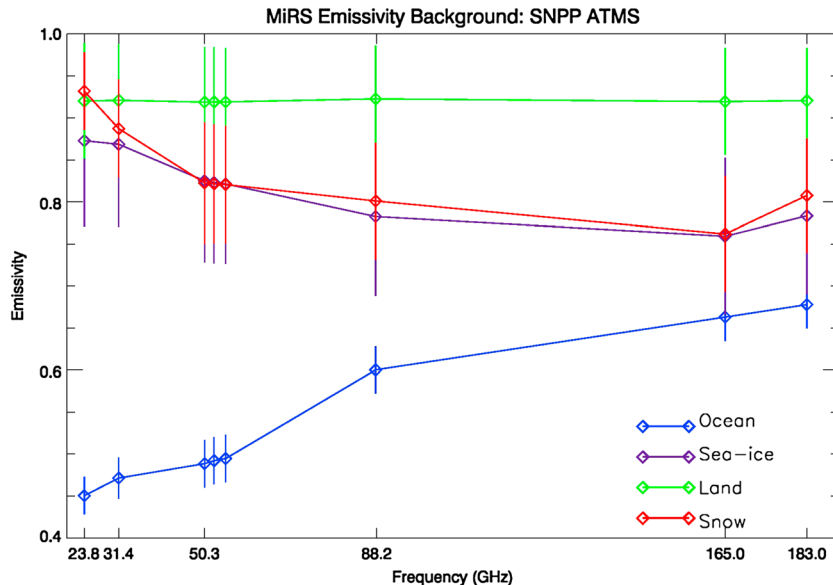


**Figure 3.** Background emissivity spectra by surface type for SNPP/ATMS, along with standard deviation.

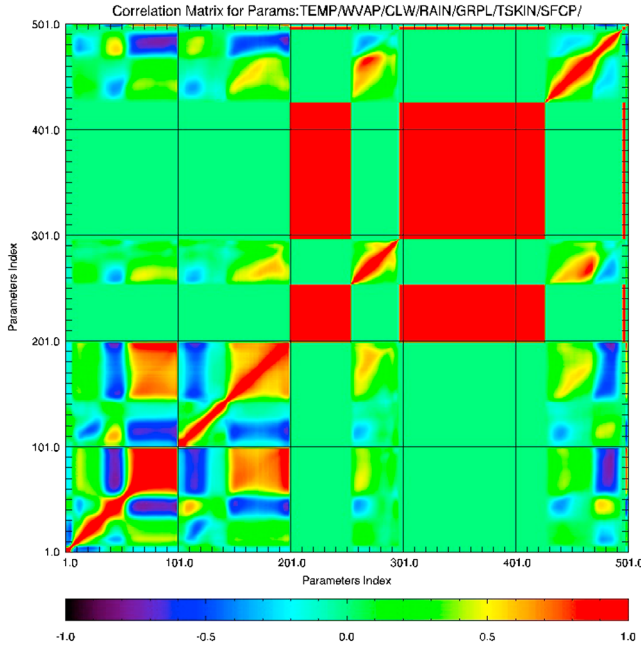


**Figure 4.** Correlation matrix for MiRS geophysical parameters used in the 1DVAR system: 1–100, temperature; 101–200, water vapor; 201–300, cloud; 301–400, rain; 401–500, ice; 501, skin temperature.

retrievals for SNPP/ATMS, including surface pressure. This is done in order to keep independence between the geophysical background covariance and the radiometric error covariance, a necessary condition for the validity of the variational assimilation/retrieval approach. The mean values of the background used in MiRS have been the subject of a recent upgrade. They are based on a geographically and seasonally distributed mean climatology that also accounts for the diurnal cycle variation.

## 5. Atmospheric Parameters Assessment

[12] The algorithm solves for the atmospheric contribution to the measurements by retrieving the temperature and moisture profiles. The total precipitable water (TPW) is then simply a vertical integration of the moisture profile. The assessment presented in this section focuses on the comparison to European Center for Medium-Range Weather Forecast (ECMWF) analyses as well as performances obtained using collocations with ground-based radiosondes.

### 5.1. Comparing to ECMWF

[13] In this section, we compare sounding products and TPW to the European Center for Medium-Range Weather Forecast (ECMWF) analyses in both clear-sky and precipitating conditions. The temperature sounding retrieval is provided

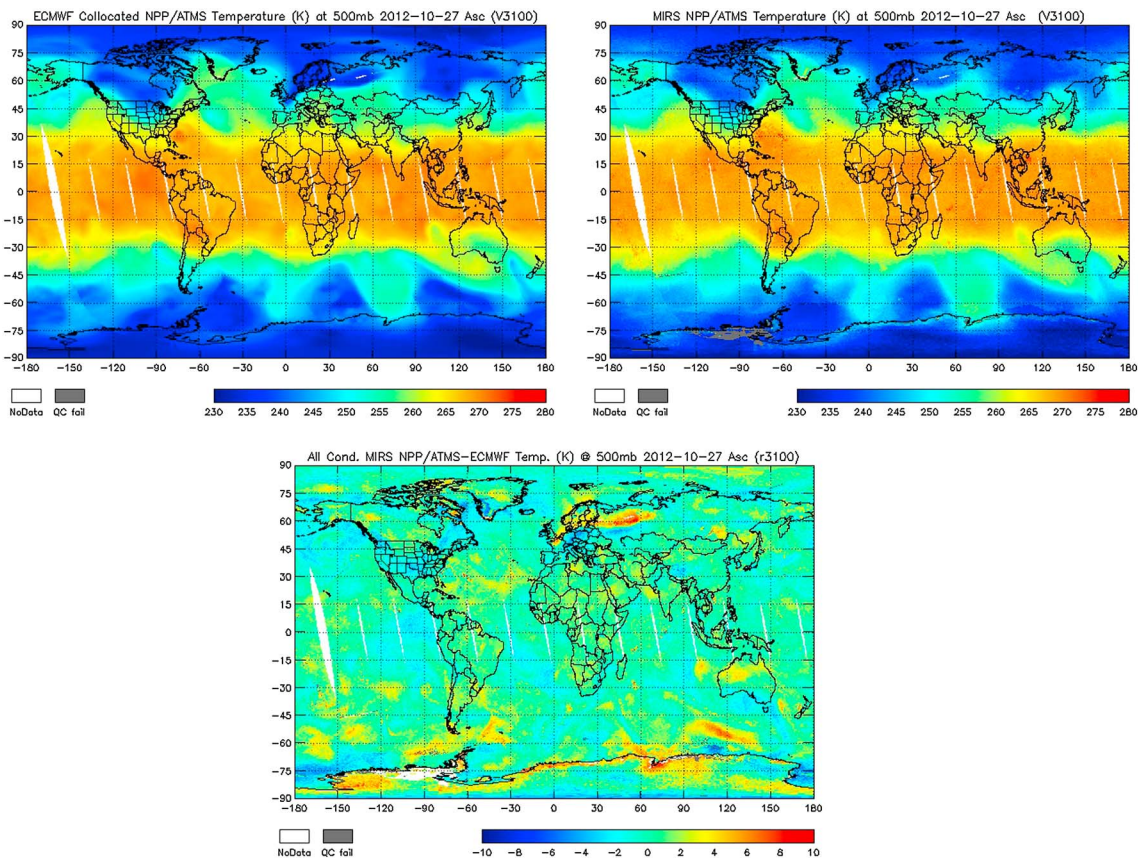


**Figure 5.** (top right) MiRS-retrieved and (top left) ECMWF analysis 500 hPa temperature along with (bottom) the difference field for case day 27 October 2012.

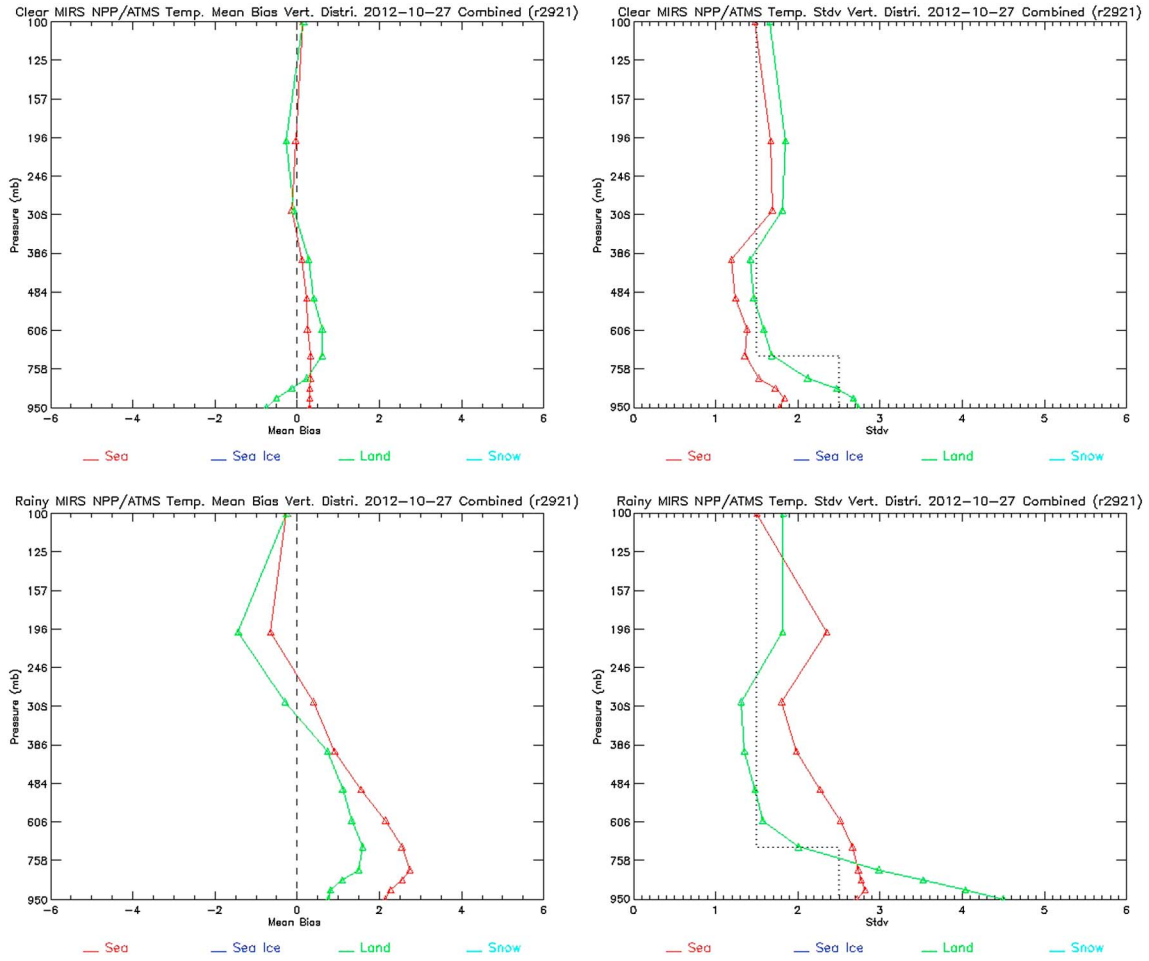


**Figure 6.** MiRS temperature (left) mean bias and (right) standard deviation over both land (green) and ocean (red) surfaces in (top) clear-sky conditions, compared to ECMWF analysis. (bottom) The same performances are shown for precipitating conditions.

at 100 atmospheric layers from the surface to 0.01 hPa over all surfaces, though only the retrievals over ocean surfaces are declared operational at National Oceanic and Atmospheric Administration (NOAA)/National Environmental Satellite, Data, and Information Service (NESDIS). Figure 5 shows an example of a comparison of the MiRS-retrieved 500 hPa temperature to ECMWF analysis for 27 October 2012, while Figure 6 shows mean bias and standard deviation over both land and ocean in both clear-sky and precipitation conditions.

[14] These figures highlight the performances of the ATMS temperature profiles, capturing all features at synoptic scale with almost no coverage gap (using only 1 day, ascending only, orbits). The statistical performances in clear and cloudy conditions are deemed to meet requirements, especially given that these errors also include time and space collocation errors, representativeness errors, and ECMWF analysis errors. These errors are expected to explain roughly 30% of the uncertainties shown here. The performances degrade as expected in exclusively rainy conditions (Figure 6, bottom). This degradation is more pronounced over land than over ocean. Over land, the emissivity is highly varying in normal conditions and become even more so when rain is falling, compounding the difficulty of retrieving atmospheric parameters in these conditions, especially at lower layers.

[15] The same statistical analysis is performed for the water vapor sounding products from MiRS SNPP/ATMS against ECMWF analysis. Figure 7 shows the 500 hPa water vapor fields from MiRS, ECMWF, and the difference MiRS-ECMWF from 16 September 2013. Figure 8 shows the water vapor profile mean bias and standard deviation from the surface to 200 hPa for clear-sky and precipitating conditions for the same day. Note that the water vapor retrievals are officially declared operational at NOAA/NESDIS only in clear/cloudy skies over both land and ocean (not in precipitating conditions), but the initial assessment of the integrated water vapor in precipitating conditions over ocean has shown promising performance (not presented here). Similarly to temperature, the moisture profiles are found to correlate very well with ECMWF global analyses, and statistically, the performances are found to be very good. The moisture uncertainties/errors due to collocation, representativeness, and analyses are deemed to represent around 40% of the overall statistics presented here. It is worth noting that in a number of cases, positive and negative differences (see Figure 7) are juxtaposed (indicated by the blue/red features in the map of the differences), usually indicating a placement shift in the NWP moisture analysis. This is either due to shift in the NWP forecast used as first guess or to interpolation

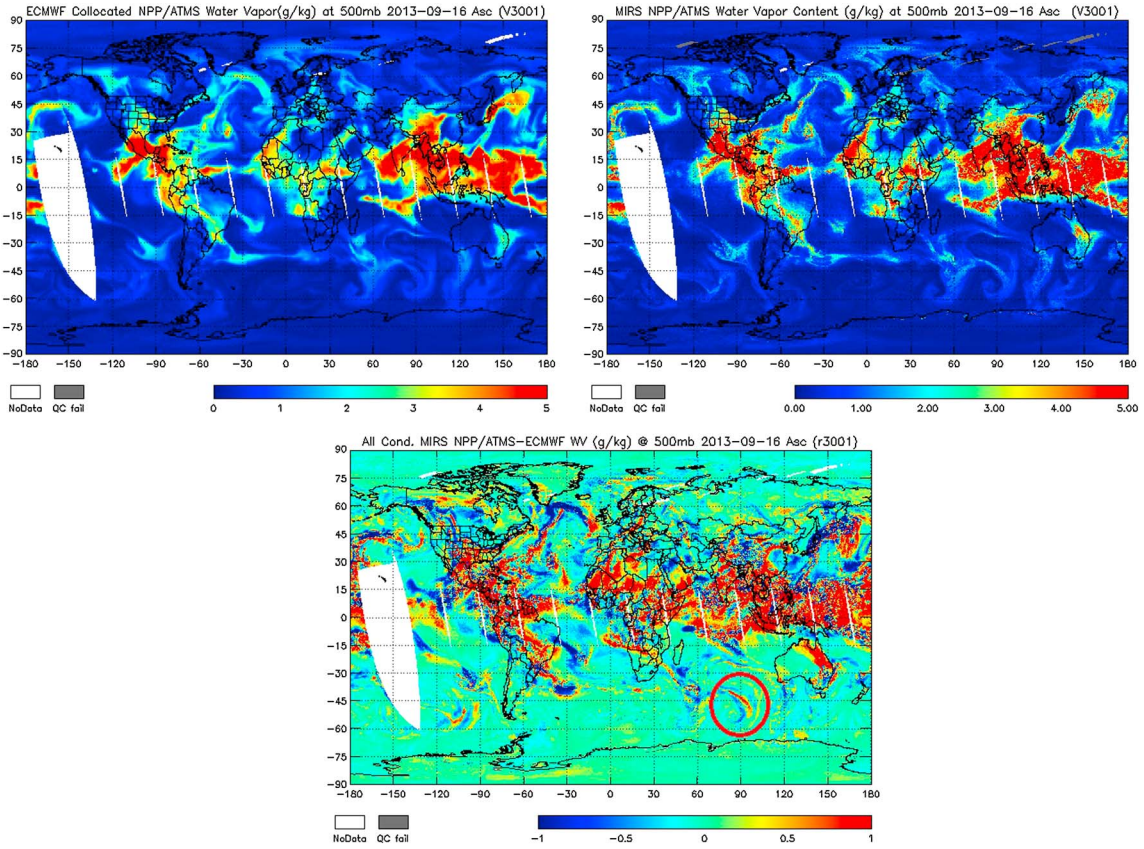


**Figure 7.** (top right) MiRS retrieved and (top left) ECMWF analysis 500 hPa water vapor along with (bottom) the difference field for case day 16 September 2013. Note that the statistical performances of the moisture retrieval are partially due to misplacement errors, highlighted by positive/negative difference features (such as the one highlighted with a circle).

errors employed to collocate analyses to the satellite retrievals. In other words, the amplitude of the analysis might be close to correct (as indicated in the moisture maps themselves), but its geographical placement might be slightly shifted, therefore generating this seesaw difference pattern. This aspect is believed to partly explain the statistics of the moisture performance.

[16] This assessment of the performances shows that MiRS-based temperature and moisture profiles from SNPP/ATMS are of good quality and compare well with ECMWF analyses, which assimilate many more sounding measurements including radiosondes and in situ sounders. The evolution of these temperature and moisture biases and standard deviations for all surfaces and for all layers are continuously monitored (not shown here). These performances are found to be very stable in time.

[17] The MiRS total precipitable water (TPW) is a simple integration performed over the water vapor column. The SNPP/ATMS TPW is valid over all surfaces and is declared operational at NOAA/NESDIS over both land and ocean surfaces, including snow- and ice-covered surfaces as well as coastal areas [Boukabara et al., 2011]. Figure 9 shows maps of the TPW calculated from MiRS and ECMWF analysis and the difference field from 27 October 2012. The same figure shows the scatterplot comparing the TPW retrieval and analysis. A summary of the TPW performances for MiRS SNPP/ATMS is shown in Table 1 for retrievals in

nonprecipitating conditions. These performances are deemed good and comparable to performances obtained with MetOp and POES microwave sounders. It is, however, worth mentioning that the almost global coverage attained with ATMS has very little orbital gap. This provides a significant added value for hurricane and other extreme weather events monitoring by ATMS. The other advantage of ATMS that is not visible from the maps shown here is the increased temporal resolution of the measurement from ATMS over the areas where the wider swaths overlap.

[18] In order to get a sense of the uncertainty in the analysis itself, used here as a reference, an assessment of the differences between ECMWF and the Global Data Assimilation System (GDAS) analyses was undertaken. It shows that differences exist even though they assimilate roughly the same conventional and satellite observations. Figure 10 shows the difference between GDAS and ECMWF 500 hPa temperature as well as differences in TPW when both analyses are collocated to the ATMS observations for 27 October 2012. Differences in temperature up to 1 K and standard deviation of less than 1 K were found for that day. The water vapor differences were more pronounced, especially for the high altitudes where relative discrepancies of more than 50% were found for layers above 500 hPa. This gives us a certain measure of what is the expected error in the analyses being used here for the assessment of the MiRS retrievals.

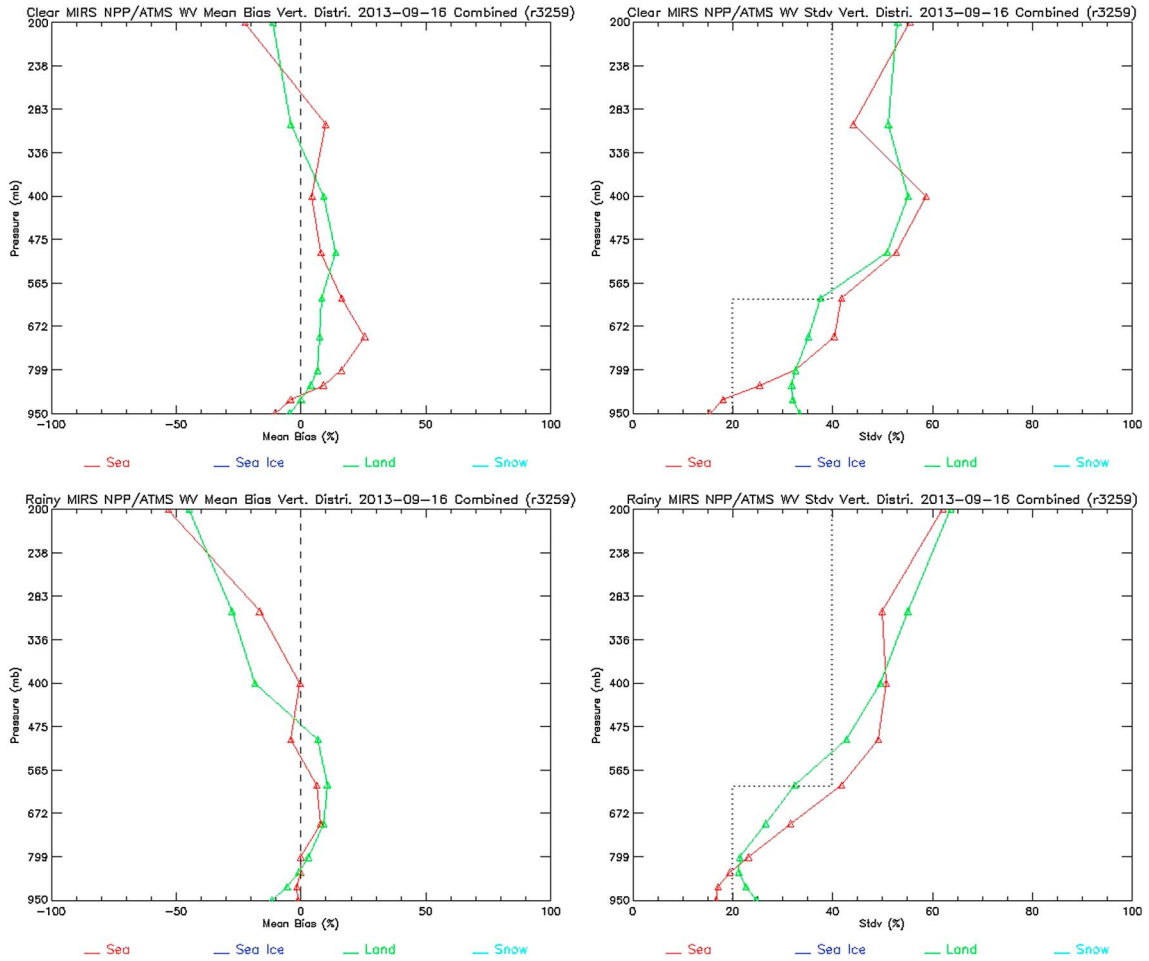


**Figure 8.** MiRS water vapor (left) percentage mean bias and (right) percentage standard deviation over both land (green) and ocean (red) surfaces in (top) clear-sky conditions, compared to ECMWF analysis. (bottom) The same performances are shown for precipitating conditions.

## 5.2. Comparing to Radiosondes

[19] Performances of MiRS sounding products have also been computed against ground-based measurements. In this section, we highlight the performances of both temperature and water vapor sounding from MiRS as compared to radiosondes. We will also compare these results with other performances of MiRS when applied to POES and MetOp AMSU-A/MHS sensors.

[20] SNPP/ATMS data were collocated with radiosondes for the period from July 2013 to September 2013 with collocation criteria of  $\pm 5$  h and  $\pm 1^\circ$  [Reale et al., 2012]. A similar record covering the same period exists for other sensors processed by MiRS, including NOAA 19 and MetOp-A AMSU-A/MHS. Therefore, the number of collocations used to compute the statistics are comparable, roughly about 22,000 for SNPP and NOAA 19 since they are in a similar afternoon orbit and 27,000 for MetOp-A. The statistics are remarkably similar showing the robustness of the collocation data sets and the consistency of the algorithm applied to same or similar sensors with only slight differences near the surface and tropopause regions. Figure 11 shows the temperature sounding bias and standard deviation for SNPP, NOAA 19, and MetOp-A over both ocean and land surfaces,

when compared to radiosondes. The collocated scenes contain those from all weather conditions (as long as the algorithm converged), and no filtering is performed on coastal sondes which MiRS may classify as either ocean or land surface depending on the dominant signal (land fraction). The statistics for SNPP temperature sounding are typically similar to those of NOAA 19. This is expected since the two satellites are on close orbits with an afternoon local crossing time, and therefore their statistics are likely based on the same geophysical situations. Temperature soundings over ocean and land from both sensors show less than 1 K bias in the troposphere and roughly 2 K standard deviation except for near the surface and tropopause. A slight difference between the SNPP and MetOp-A performances could be seen and could

**Table 1.** Performance Summary of MiRS TPW for SNPP/ATMS Over All Surfaces and in Clear-Sky Conditions

	Bias (mm)	SD (mm)	Corr.	RMSE (mm)
Ocean	0.46	2.55	0.98	2.59
Land	0.48	4.47	0.95	4.50
Sea ice	0.42	1.28	0.82	1.35
Snow	0.25	0.89	0.93	0.92

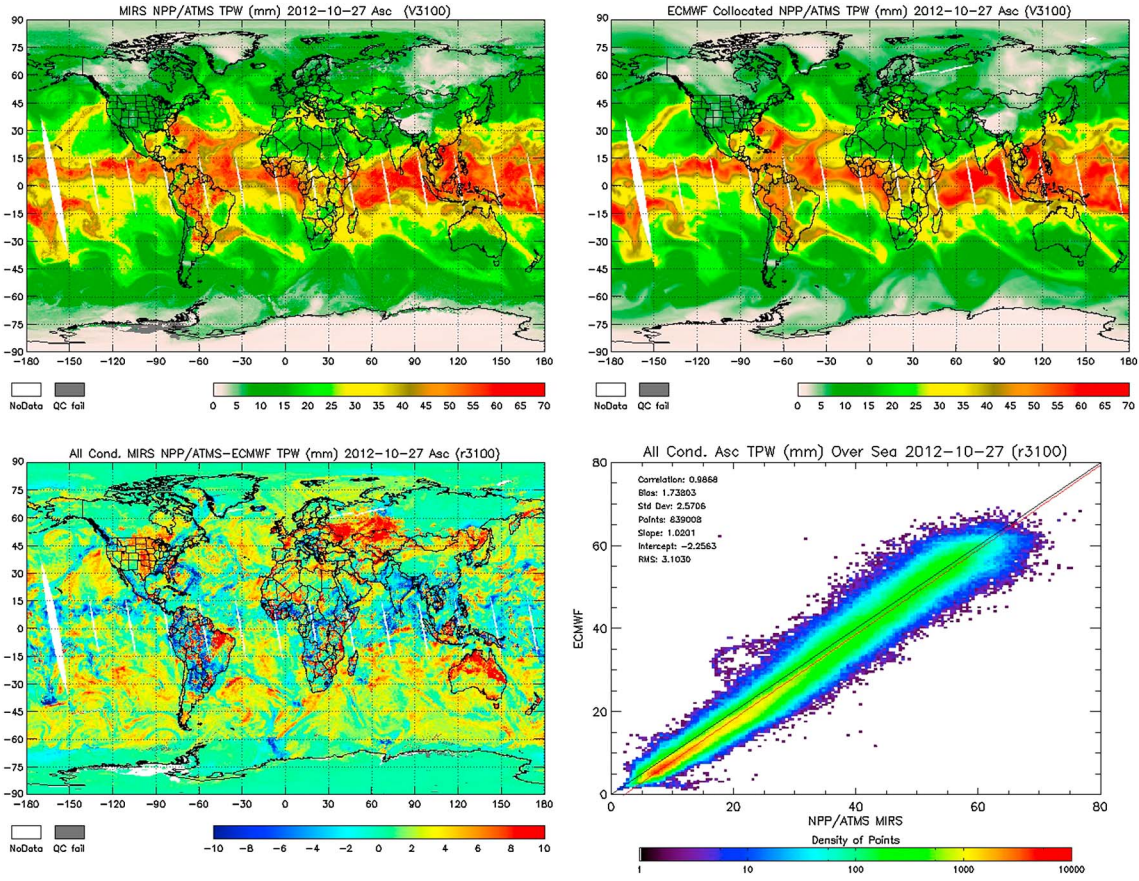


**Figure 9.** Total precipitable water from (top left) MiRS, (top right) ECMWF analysis, and (bottom left) MiRS-ECMWF difference for 27 October 2012. (lower right) Scatterplot of MiRS TPW from SNPP/ATMS versus ECMWF analysis for 27 October 2012 over ocean surfaces.

largely be explained by the different sample sizes and the differing orbits. MetOp-A is in the morning orbit. It is worth noting that ATMS does have an extra temperature sounding channel at 51 GHz, which was expected to slightly increase the sounding accuracy in the lower-middle troposphere, but this does not seem to be the case for this comparison. To understand why that is the case, we note that the physical approach adopted here includes a geophysical constraint using the background covariance matrix, which forces the vertical layers to be consistent, minimizing the potential added value of an *extra* channel. It is speculated, however, that the extra channel might have its importance, not necessarily in terms of statistical performances but in resolving individual cases, particularly in cloudy and rainy conditions where the profile will likely depart from the average-based background.

[21] Figure 12 shows the water vapor sounding bias and standard deviation in percentage for the same sensors and collocation record. Again, over both ocean and land surfaces, the soundings performances from ATMS are statistically similar to those from the heritage sensors. The ATMS performances appear slightly better in the mid-upper troposphere. All sensors appear to have a dry bias near the surface over both ocean (10%) and land (10–20%), while a slight moist bias exists around 600–700 mbar (10–30%), although less bias is exhibited by SNPP. Error standard deviation near the surface is approximately 20–25% over both ocean and land and increases to 60% in the middle to upper troposphere.

The moisture sounding error is expressed quantitatively in terms of TPW percentage error in Table 2 for each sensor. The radiosonde TPW is computed the same way as MiRS retrieved TPW through a vertical integration of the water vapor profile. Performances between SNPP and NOAA 19 are strikingly similar, showing a moist bias of 7–8% over ocean and 2–5.5% over land, respectively. Percent standard deviation is almost identical at ~15.5% over ocean and 23% over land. For MetOp-A the percent bias is close to that of SNPP but with lower standard deviation of 13.7% and 22% over ocean and land, respectively, consistent with the results of the moisture profiles.

## 6. Surface Products Assessment

[22] The surface skin temperature and the effective surface emissivity (at all channels) are part of the state vector being retrieved in MiRS. The advantage of using the emissivity

**Table 2.** Percent Bias/Standard Deviation (mm) of MiRS TPW Compared to Radiosonde for SNPP, NOAA 19, and MetOp-A Collocations Between 1 July and 1 September 2013

	SNPP Bias/SD (mm)	NOAA 19 Bias/SD (mm)	MetOp-A Bias/SD (mm)
Ocean	7.25/15.40 (%)	8.26/15.69 (%)	8.89/13.7 (%)
Land	2.39/23.65 (%)	5.68/23.76 (%)	2.57/22.11 (%)

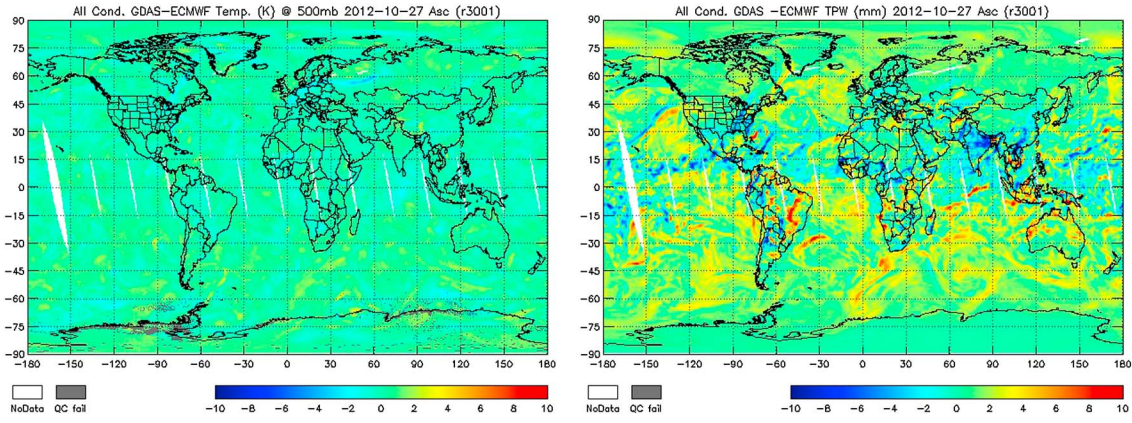


**Figure 10.** Difference fields between GDAS and ECMWF 500 mbar (left) temperature and (right) TPW for 27 October 2013. The analysis fields are collocated in time and space to the SNPP/ATMS observations. Differences between the analyses exist. For temperature, biases up to 1 K and standard deviation of less than 1 K are found. For water vapor, differences are more pronounced as could be seen in the TPW figure (right) but are especially high for high altitudes where differences of more than 50% are found above 500 hPa.

in the state vector was shown to extend the validity of the retrievals to all surfaces [Boukabara et al., 2010; Boukabara, 2011] since the only difference between retrieval over ocean, land, snow, and sea-ice surfaces is the spectral shape of the obtained emissivity vector. This section presents the results of the assessment of both the Tskin and the emissivity.

### 6.1. Assessing ATMS Surface Emissivity

[23] The assessment of the SNPP/ATMS-based dynamically generated emissivities, over non-ocean surfaces, will rely on the comparison of MiRS-based emissivities with emissivities retrieved analytically using collocations between NWP analyses and actual measurements of ATMS. In this collocation, all parameters would be known and the only unknown is the emissivity which could be inverted using the following equation [Prigent et al., 2008; Norouzi et al., 2012].

$$\varepsilon = \frac{\left( \frac{T_B - T^\dagger}{\Gamma} - T^\dagger \right)}{T_s - T^\dagger}$$

[24] Where  $T_B$  is the brightness temperature,  $\varepsilon$  the emissivity we would like to compute,  $T_s$  the surface temperature,  $T^\dagger$  and  $T^\ddagger$  the upwelling and downwelling radiances, respectively, and  $\Gamma$  is the total atmospheric transmittance. Over ocean surfaces, the comparison is performed against Fast microwave Emissivity Model (FASTEM) [Liu et al., 2011] model emissivities that take wind speed inputs from the NWP analyses. Because the land emissivity is the official product produced operationally, the following results will focus on the land, sea-ice, and snow emissivities performances. This is done in exclusively clear-sky conditions since the transmittance, when cloud is present, cannot be simulated properly because of the lack of accurate cloud input information from the NWP analyses.

[25] Figure 13 shows the emissivity performances for a single day, 6 March 2013, as retrieved over land and snow from SNPP/ATMS data. It is clear that emissivity is capturing the major surface signals. The Amazon River lower emissivity could clearly be seen in the retrieved emissivity. The known

angle-varying emission of the desert surfaces is clearly captured as well. The lower and spectrally decreasing-with-frequencies emissivities over snow surfaces (Eurasia and North America) is also well captured in the emissivity. The emissivity vector inverted by the algorithm could be interpreted, in a sense, as equivalent to the brightness temperatures but with the atmospheric signal having been removed. This signal of the emissivity is then converted into surface parameters. Over cryospheric surfaces (snow and ice), the emissivity is converted into snow water equivalent and sea-ice concentration, respectively. In terms of emissivity performances, the biases for both land and snow are around or less than (1%), respectively, which is consistent with other results obtained from other sensors and using other methodologies such as physical land emissivity models [Ferraro et al., 2013; Weng et al., 2001]. Correlation for both surface types hovers around 0.8, and the standard deviation is 3 or 4%, respectively. It is worth noting that these statistics include (1) errors due to the inputs that served in the computation of the analytical emissivity, in particular the temperature and moisture profiles but also the skin temperature; (2) the limitations of the analytical approach which is valid only over specular surfaces; (3) errors due to the spatial and temporal interpolations performed to the analyses to collocate them with the ATMS measurements; and finally (4) errors due to absorption modeling uncertainties in these frequencies which lead to inaccurate transmittance and down/upwelling radiances. It is estimated, based on assessing the retrieval algorithm performances in simulation mode (not shown here), that the algorithm accuracy for emissivity is actually 1 to 2% depending on the frequency and surface type. One added value of the approach adopted here is the inversion of the entire emissivity spectrum, allowing for the use of the entire spectral shape to better determine the surface products that are determined based on the emissivity. Table 3 shows the performances of the emissivity for select channels for different surface types.

### 6.2. Assessing ATMS Surface Skin Temperature

[26] The assessment of skin temperature performances relies on both global comparisons with Numerical Weather Prediction (NWP) analyses, interpolated to the ATMS footprints, and on

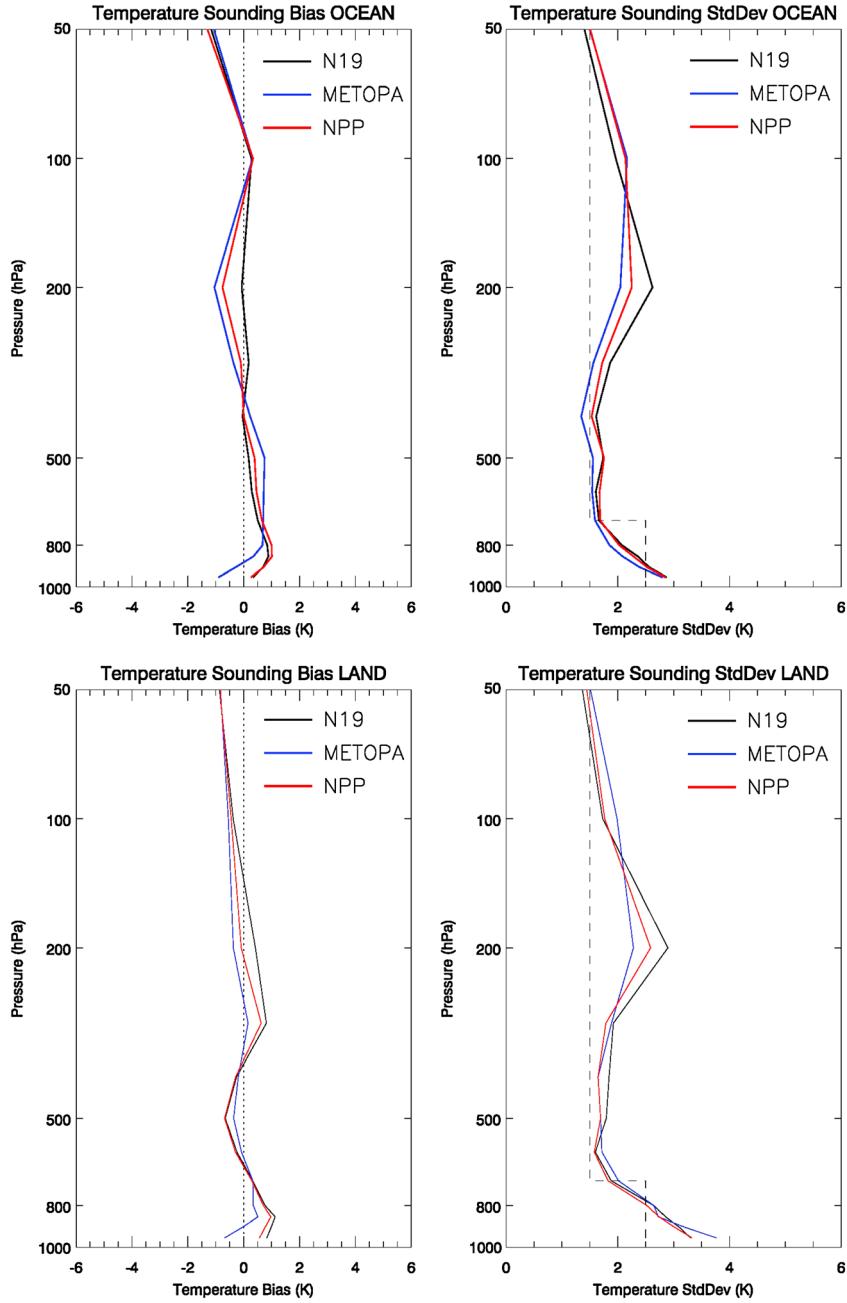


**Figure 11.** Temperature sounding bias and standard deviation over (top) ocean and (bottom) land for MiRS applied to NOAA 19 (black), MetOp-A (blue), and SNPP (red). Statistics are computed using global radiosondes as reference.

comparisons with Surface Radiation (SURFRAD) network-based ground measurements of surface temperatures. For this assessment of surface temperature, it is important to calibrate the expectation because of the difficulty in achieving an apple-to-apple comparison. Indeed, NWP analyses usually refer to ground surface temperature, while spaceborne sensors measure the temperature at the surface boundary, and the depth of that boundary depends on both the radiometric characteristics of the sensor (i.e., frequency therefore penetration depth, viewing angle, footprint size, and antenna pattern) as well as on the characteristics of the surface itself (presence of vegetation, trees, topography, and presence of water bodies). For conciseness but also because of known deficiencies

in the analyses in the estimation of the surface temperature, only the ground-based assessment of MiRS-based skin temperature is presented in this study. Table 4 shows the list of the SURFRAD stations used in this study. The following discussion will present how the performances were obtained and will then compare them to performances published in previous studies. It also discusses the expected performances based on simulated data and provides an overview of the errors impacting the results. Since SURFRAD collects data every minute, the ATMS data are collocated almost perfectly in time. The spatial collocation uses an 11 km threshold to identify a matchup. Figure 14 summarizes the performances of the Land Surface Temperature (LST) as measured over snow-free

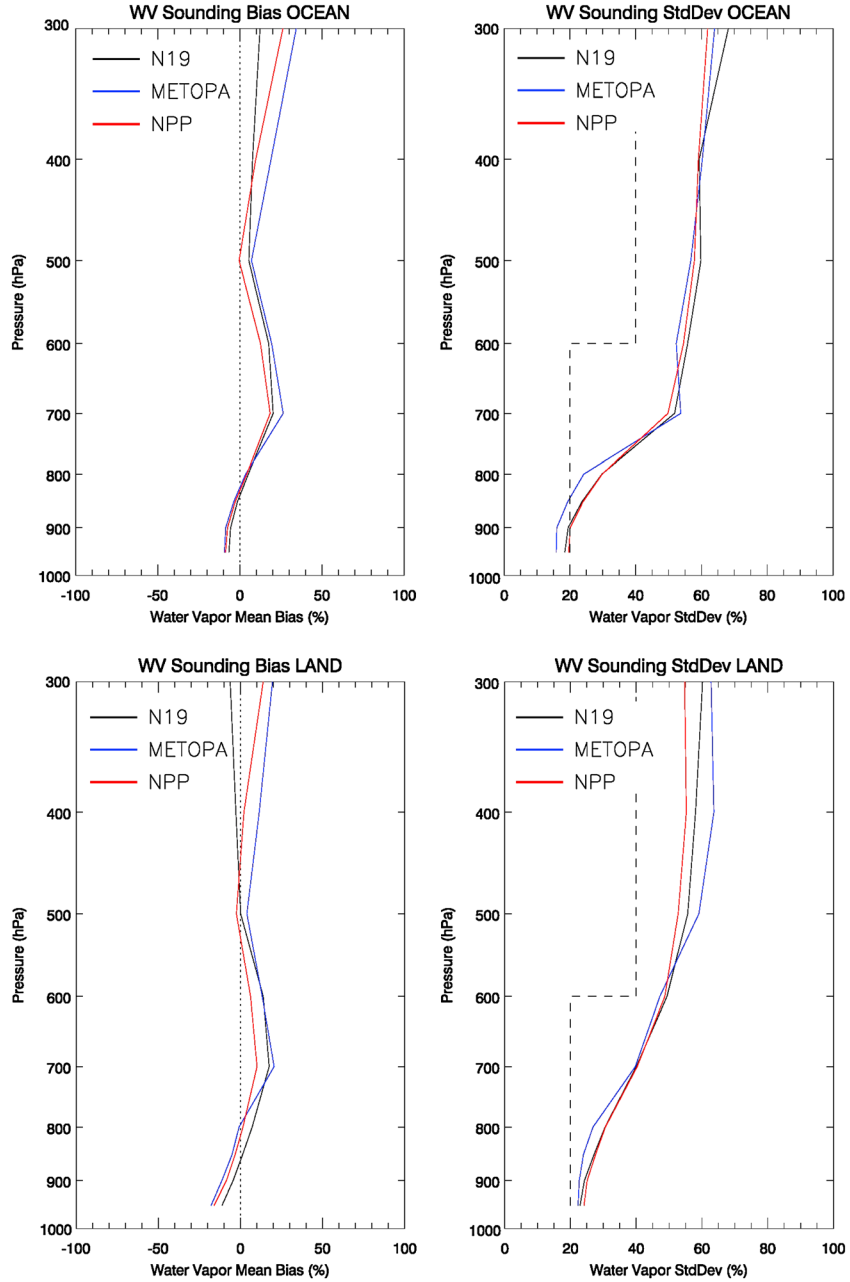


**Figure 12.** Water vapor sounding bias and standard deviation over (top) ocean and (bottom) land for MiRS applied to NOAA 19 (black), MetOp-A (blue), and SNPP (red). Statistics are computed using global radiosonde as reference.

and snow-covered surfaces. The performances, summarized in Table 5, range from 3.8 to 7 K (in terms of standard deviation) and between 0.6 and 0.9 (in terms of correlation) depending on the collocation site and its vegetation characteristics. The overall correlation is 0.8, and the overall standard deviation is 5 K. These performances are lower (errors higher) than those published by *Holmes et al.* [2009], where the standard error of estimate presented varied between 2.3 and 4.5 K, depending on the vegetation coverage. That study was performed using a slightly different frequency (37 GHz) than available with the ATMS (mainly 23 and 31 GHz) and using a conical-scanning sensor, as opposed to ATMS cross-track scanning geometry. Another study by *Parinussa et al.* [2008], using the same Ka

band frequency and the same conical-scanning geometry, reported a standard error deviation between 2.1 and 4.9 K. To understand these real-data performances better, an assessment against expected performances was performed, using simulated data and a generic regression-based algorithm for the inversion. For completeness, this simulation of the performances was done for both the ATMS configuration and the Special Sensor Microwave Imager/Sounder (SSMIS) configuration (using the conical-scanning geometry and the 37 GHz frequency, as opposed to the ATMS cross-track geometry and 31 GHz). This was done in order to double check that the performances obtained in this study are consistent with previously published results where the Advanced Microwave

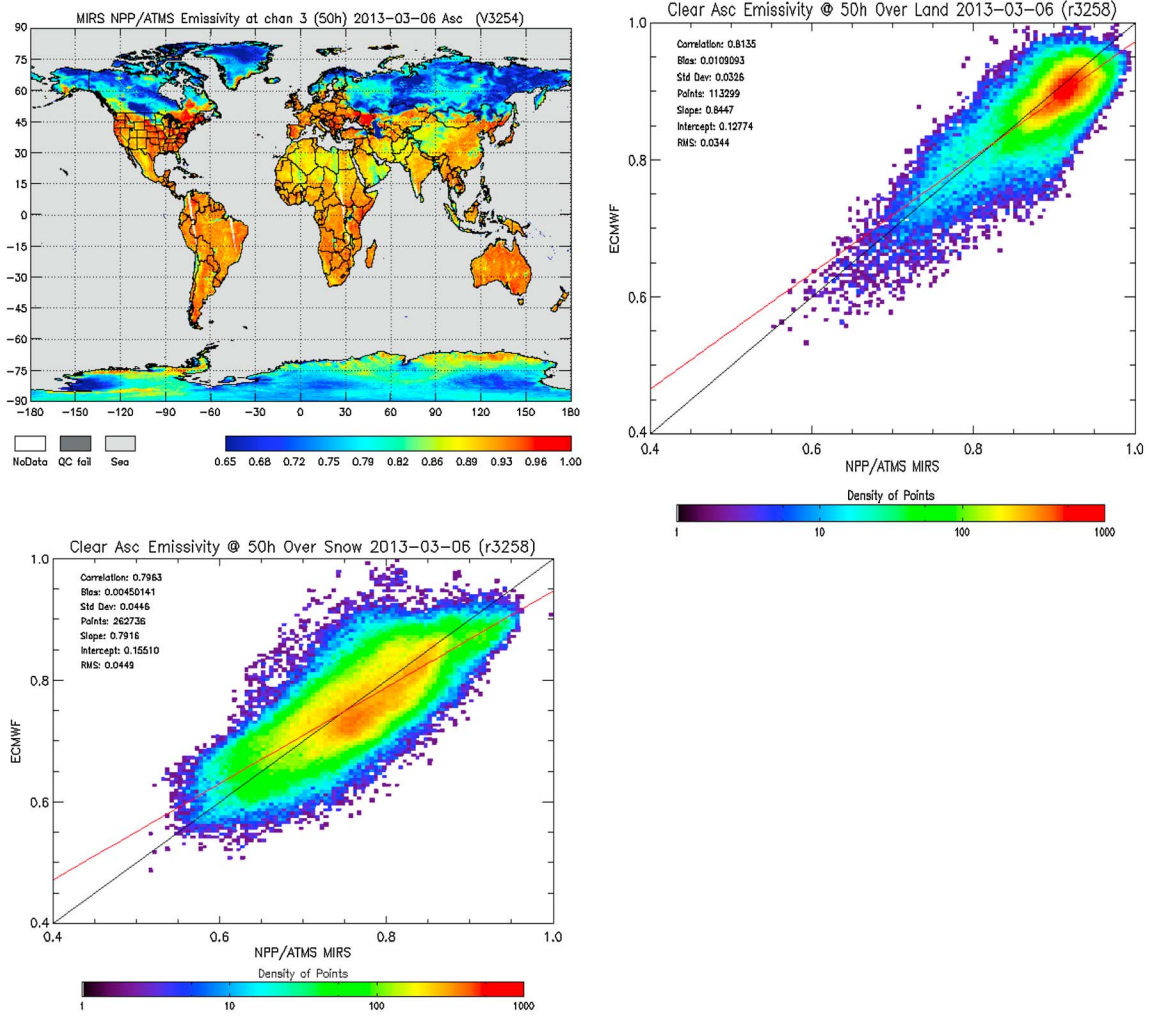


**Figure 13.** (top left) Illustration of the emissivities at channel 3 (50.3 GHz) over non-ocean surfaces and statistical comparison with the analytical emissivities, stratified by (bottom left) snow and (top right) nonsnow covered land.

Scanning Radiometer for EOS (AMSR-E) or the SSMIS configurations were used. It was found that the SSMIS configuration leads to consistency with published results, with a standard error of about 3.5 K if RTM uncertainty and instrument noise are added (it drops to 3.1 K if only noise is added). The expected performances when using simulated ATMS configuration leads to 4.7 K and 4.1 K (depending on whether both noise and RTM errors are added or only noise), which is also consistent with the results found in this study when comparing MiRS-based LST with SURFRAD (5 K overall standard deviation). Knowing

that the performances of LST as retrieved by real ATMS data are negatively impacted by (1) the time and space collocation errors, (2) the representativeness error between satellite footprint and point ground measurement, (3) the mixed surface type within the sensor footprint, (4) the uncertainty of the ground reference measurements themselves, etc., it is deemed that the slight increase in the standard deviation, from the simulation-based expected performance, is to be expected. Another aspect that is expected in this comparison is the systematic bias between the SURFRAD measurements and the satellite-based

**Table 3.** Summary of Single-Day-Based Statistics of the MiRS-ATMS Emissivity Performances in Terms of Bias, Standard Deviation, and Correlation When Compared to the Analytical Emissivity<sup>a</sup>

	23 GHz	31 GHz	50.3 GHz	88 GHz
Land	Bias: 0.01 SD: 0.02	Bias: 0.01 SD: 0.02	Bias: 0.01 SD: 0.03	Bias: 0.01 SD: 0.02
Snow	Correlation: 0.91	Correlation: 0.91	Correlation: 0.80	Correlation: 0.86
	Bias: 0.02 SD: 0.03	Bias: 0.02 SD: 0.03	Bias: 0.01 SD: 0.04	Bias: 0.02 SD: 0.03
	Correlation: 0.92	Correlation: 0.91	Correlation: 0.81	Correlation: 0.86

<sup>a</sup>Performances are stratified by surface type.

**Table 4.** Description of the Location and Type of Surface Where SURFRAD Stations Are Situated

Geolocation and Surface Type of the Six SURFRAD Stations			
No.	Site Location	Latitude ( $^{\circ}$ N)/Longitude ( $^{\circ}$ W)	Surface Type
1	Bondville, IL	40.05/88.37	Cropland
2	Fort Peck, MT	48.31/105.10	Grassland
3	Goodwin Creek, MS	34.25/89.87	Deciduous forest
4	Table Mountain, CO	40.13/105.24	Cropland
5	Desert Rock, NV	36.63/116.02	Open shrub land
6	Pennsylvania State University, PA	40.72/77.93	Mixed forest

LST. This indeed varies between  $-1.2$  K and  $-4.7$  K. To understand this bias, it is important to note that the SURFRAD ground stations measure high quality of upwelling and downwelling long-wave radiations, which is then transformed into an LST measurement using estimates of infrared spectral region emissivity [Yu *et al.*, 2009]. This is expected to generate a systematic bias in the comparison to the ATMS-based LST because of (1) the uncertainty in the estimate of the IR emissivity but also because (2) the infrared and microwave measurements of LST capture different depths within the surface. If the surface is not thermally homogeneous, the correlation between Microwave and Infrared LST gets degraded (see Table 5). The overall bias is found to be around  $3.5$  K in line with the expected IR/MW surface-depth sensing discrepancy. This is also consistent with differences between IR-based Moderate Resolution Imaging Spectroradiometer LST and MW-based LST published by Parinussa *et al.* [2008], where discrepancies were reported to be consistent across all sites and exhibited a standard error of  $\sim 4$  K.

## 7. Hydrometeors and Rainfall Assessment

[27] The surface rainfall rate in this algorithm is generically determined through a function developed offline relating the integrated amounts of the hydrometeors to the rain rate. More detail can be found in Iturbide-Sánchez *et al.* [2011]. Because of this, and because of the difficulty obtaining ground measurements of (RWP) and (IWP), the assessment of the surface rainfall rate represents an indirect assessment of the quality of the hydrometeors retrieved by MiRS. This assessment uses comparisons against both ground-based radars and rain gauge observations. The time series presented here show the evolution of the rainfall rate performance from early to more mature stages, highlighting the impact of improvements carried out during the Cal/Val phase.

### 7.1. Comparing to Climate Prediction Center Analyses

[28] SNPP/ATMS rainfall rate has been collocated and compared over the contiguous United States (CONUS) against the 24 h ( $-12:00$  to  $12:00$  UTC) gridded ( $0.5 \times 0.5^{\circ}$ ) rain gauge analysis NOAA/National Centers for Environmental Prediction (NCEP) Climate Prediction Center (CPC) precipitation [Chen *et al.*, 2008]. Figure 15 presents a map comparison between the MiRS SNPP/ATMS rainfall rate and the CPC precipitation.

[29] In general, the MiRS SNPP/ATMS rainfall product is able to capture precipitation patterns and intensities similar to the ones observed by the CPC precipitation. Figure 16 presents the performance of the MiRS SNPP/ATMS rainfall rate

observed after several months of daily comparisons against the 24 h CPC precipitation composite. This result also helps to compare the performance of MiRS SNPP/ATMS rainfall rate relative to other MiRS rainfall rate products from other sensors, namely, NOAA 18 and 19, MetOp-A, and DMSP F16 and F18. The precipitation composite based on observation from three sensors, NOAA 18, MetOp-A, and DMSP F16, is also shown in that time series. This composite product is expected to have the best performance due to its superior temporal and spatial coverage, as compared to accumulated precipitations based on single sensor observations.

[30] Around August 2012, one can notice that the detection of light precipitation (lower than  $1.0$  mm/h) was significantly improved for the MiRS SNPP/ATMS rainfall rate. The improvement was achieved after tightening the magnitude of the radiative transfer model error assumed for the high-frequency channels, more specifically channels 17 and 18, which are highly sensitive to the presence of precipitation. This improvement was positively reflected in other scores and statistics, resulting in an overall improvement of the rainfall rate product. The consistently better probability of detection of the MiRS SNPP/ATMS rainfall rate with respect to other MiRS rainfall rate estimates is interpreted as due to the better spatial coverage offered by the SNPP/ATMS sensor.

### 7.2. Comparing to Stage IV Precipitation Product

[31] The hourly NCEP Stage IV precipitation product [Lin and Mitchell, 2005] is a  $4$  km resolution precipitation analysis derived from hourly radar precipitation estimates and rain gauge data obtained over the CONUS. Due to the quality of this precipitation product, comparisons against the MiRS SNPP/ATMS rainfall rate have been carried out and presented in this section. For comparison purposes, it has been assumed that the Stage IV precipitation is a constant amount for an entire hour and is compared against the MiRS rainfall rate estimate that had occurred within that hour. In order to account for spatial resolution differences, the hourly NCEP Stage IV precipitation was averaged over the MiRS SNPP/ATMS rainfall rate spatial resolution (about  $15$  km).

[32] Figure 17 shows maps of collocated MiRS SNPP/ATMS rainfall rate and the hourly NCEP Stage IV precipitation.

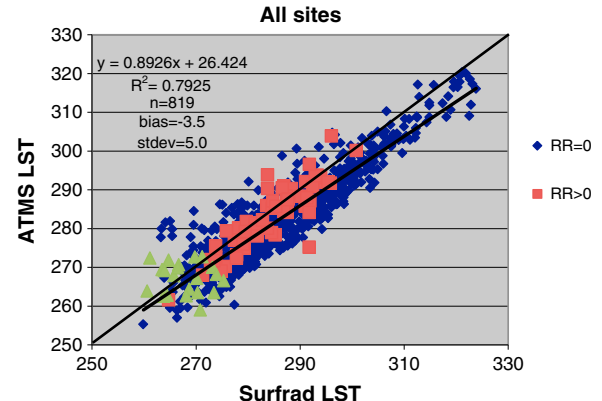


**Figure 14.** Performances of the Land Surface Temperature (LST) from SNPP/ATMS using the MiRS algorithm, as compared to all six sites of the SURFRAD. The different colors highlight the nonrainy points (blue), the rainy points (red), and the points identified by MiRS as snow-covered (green).

**Table 5.** Stratification of the LST Performance (Correlation With SURFRAD Measurements) by Station and Surface Type<sup>a</sup>

	Correlation Factor	Bias (K)	Standard Deviation (K)
Bondville IL (cropland)	0.9	-4.7	3.8
Fort Peck, MT (grassland)	0.6	-1.2	7.0
Goodwin Creek, MS (deciduous forest)	0.8	-4.6	4.7
Table Mountain, CO	0.9	-3.9	5.1
Desert Rock, NV	0.9	-1.9	4.6
Penn State University (mixed forest)	0.8	-4.0	4.0
All sites (all weather conditions)	0.8	-3.5	5.0

<sup>a</sup>Both clear and cloudy points are included. Both snow-free and snow-covered (if any) points are included.

MiRS SNPP/ATMS rainfall rate is able to handle the land-ocean transition with no discontinuities and to estimate precipitation fields over similar regions as the ones observed by the Stage IV product. Similarly to the CPC comparison, for the evaluation of the instantaneous rainfall rate, statistics and scores have been computed after daily collocations against the Stage IV precipitation product. Those results are presented in Figure 18, where the performance of the operational Microwave Surface and Precipitation Products System (MSPPS) algorithm is included. Results presented in Figure 18 show that the MiRS SNPP/ATMS rainfall rate algorithm strikes a good balance between its detection capability and the inevitable false alarms. It produces a bias close to zero and root-mean-square error (RMSE) values generally lower than 1.0 mm/h. The overall performance of the SNPP/ATMS rainfall rate estimate is comparable to the other sensors.

## 8. Cryospheric Products Assessment

[33] Official cryospheric products retrieved in MiRS are sea-ice concentration (SIC), snow water equivalent (SWE), and snow cover extent (SCE). These products are retrieved as part of the postprocessing component in MiRS in which the core retrieved products, particularly surface emissivity and surface skin temperature, are used in conjunction with precomputed catalogs that relate emissivity characteristics at each channel to the amounts of sea ice and snow water, respectively. Separate catalogs are maintained for each operational sensor processed by MiRS, including SNPP/ATMS,

to account for the instrument characteristics of each sensor (e.g., frequency, polarization, and satellite zenith angle). Further details of the postprocessing algorithms and the methodology used to generate the catalogs can be found in Kongoli et al. [2011] and Boukabara et al. [2011]. In this section, we concentrate our focus on the sea-ice concentration performance assessment by performing several qualitative and quantitative analyses. Figure 19 shows an example containing the global map of MiRS retrieved SIC on 5 February 2013, with a corresponding map of SIC obtained from the daily near-real-time product of DMSP F17 SSMIS using the NASA Team algorithm. Agreement between the two products is quite high. Another comparison can be found in Figure 20, which shows the Northern Hemisphere maps of sea-ice extent obtained from MiRS-ATMS and the National Ice Center Interactive Multisensor Interactive Snow and Ice Mapping System (IMS) for 21 February 2013. Generally good agreement is also confirmed in this comparison. The robustness of the performances is assessed quantitatively by analyzing the time series of the standard deviation, the correlation factor, the bias, and the Heidke score, using the F17-based SIC measurements as a reference. Indeed, routine and automated comparison between the MiRS SIC and that from the F17 product (using the NASA T-2 algorithm) is performed daily, with quantitative metrics calculated for all seven of the sensors on which the MiRS algorithm is run. The ATMS-based performances are therefore compared to other sensors' performances in that same analysis. These include MetOp-A and B, POES N18 and N19 AMSU/MHS sensors, and DMSP F16 and F18 SSMIS. Figure 21 shows this time series of the performance metrics versus the F17 near-real-time product for all sensors (ATMS is indicated in mustard color). The initial period during which the ATMS data were being calibrated and the MiRS algorithm was tested and tuned is highlighted, as the performance for ATMS is not expected to be optimal. Once the retrieval system was stabilized, the performance of ATMS SIC appears to be consistent with and slightly better than most of the other operational sensor products. The increased noisiness in the performance in summer 2012 is related to the melting of the Arctic ice in the warm season, which results in a more ambiguous passive microwave signal as large portions of the ice pack become wet or covered with melted water. Once the autumn freezeup and development of first-year ice commences, the performance metrics stabilize

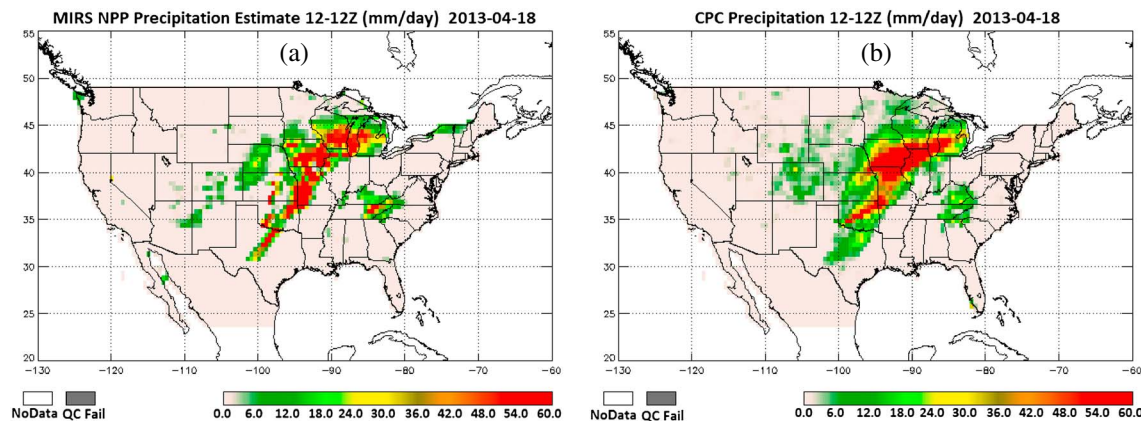


**Figure 15.** The 24 h (–12:00 to 12:00 UTC) precipitation from the (a) MiRS SNPP/ATMS rainfall rate product and the (b) CPC precipitation.

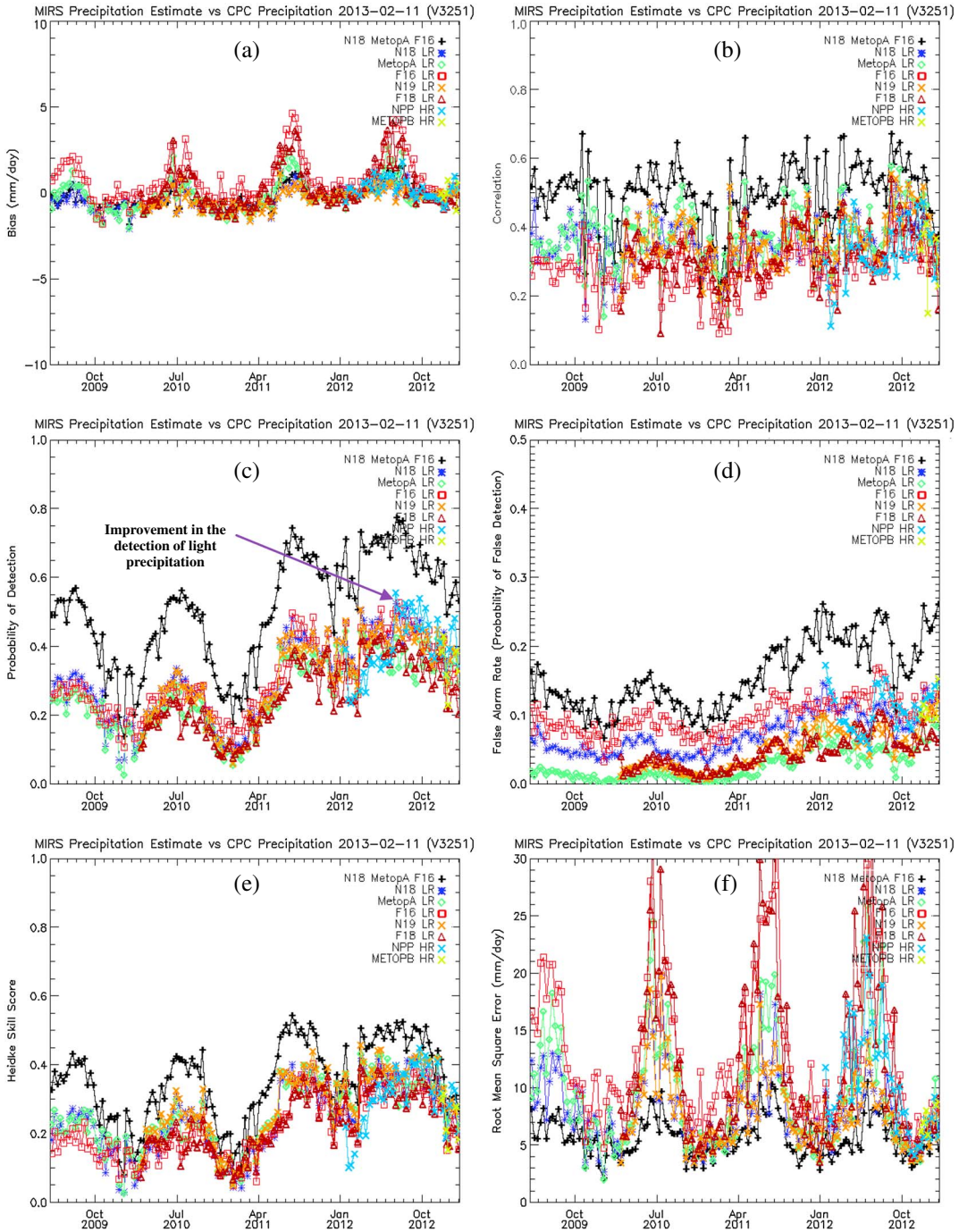


**Figure 16.** Time series of the (a) bias, (b) correlation, (c) probability of detection, (d) false alarm rate, (e) Heidke skill score, and (f) RMSE of MiRS rainfall rate products, when compared against the 24 h NOAA/NCEP CPC precipitation. LR denotes a low-resolution product (about 50 km for NOAA 18 and 19 and MetOp-A, and 75 km for DMSP F16 and F18), and HR is used to identify a high-resolution product (about 15 km for SNPP/ATMS, in light blue color, and MetOp-B, in light green).

to values seen in the previous winter season. Since the F17 product is itself a microwave retrieval, it should be considered as relative rather than an absolute reference. These results provide confidence that the SIC from MiRS/ATMS is performing well and compares favorably to other well-established SIC estimates but also that these performances are robust and slightly better than the performances obtained when applying the same MiRS algorithm to other sensors such as AMSU and SSMIS.

This added value from ATMS is attributed to the higher spatial resolution applied in the case of ATMS as opposed to the lower spatial resolution applied for the other sensors.

## 9. Conclusion

[34] We present in this study the performances obtained when applying the Microwave Integrated Retrieval System

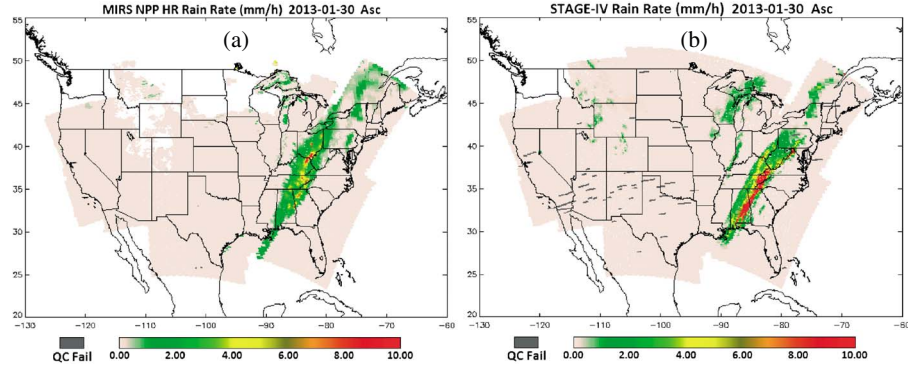


**Figure 17.** (a) The instantaneous MiRS SNPP/ATMS rainfall rate and (b) the hourly NCEP Stage IV precipitation product.

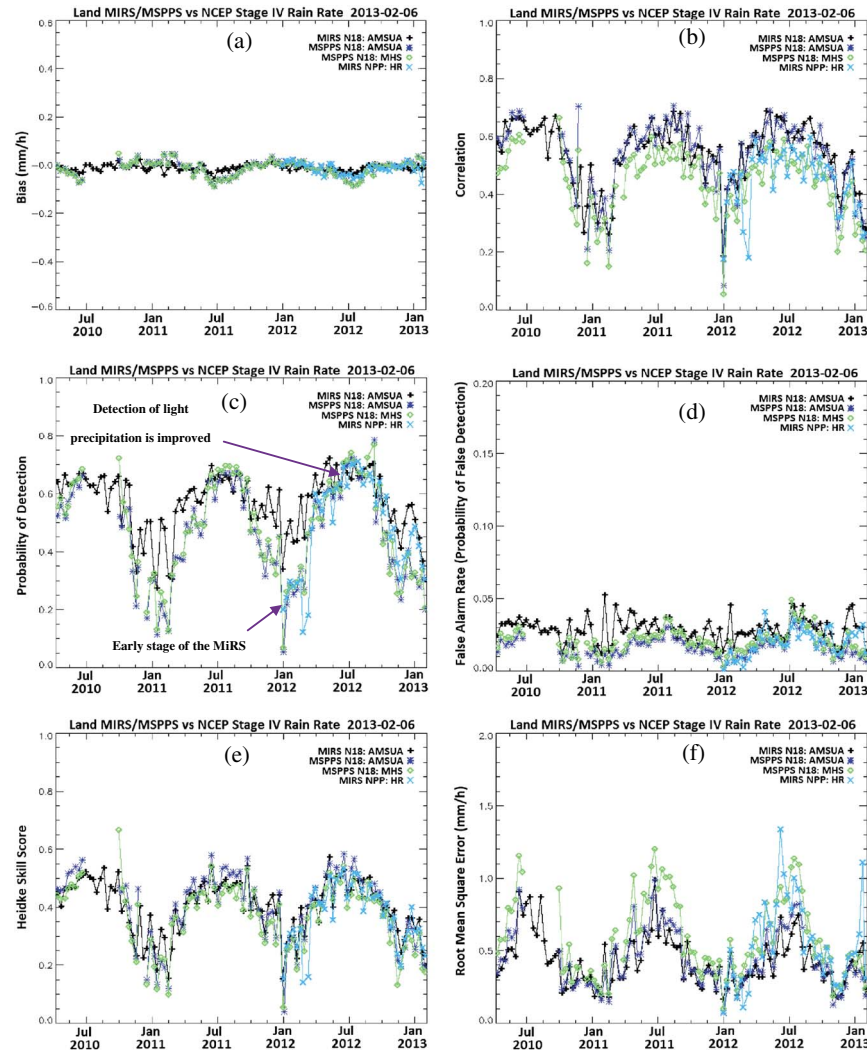


**Figure 18.** Time series of the (a) bias, (b) correlation, (c) probability of detection, (d) false alarm rate, (e) Heidke skill score, and (f) RMSE of MiRS and MSPPS rainfall rate products, when compared against the hourly NCEP Stage IV precipitation. HR is used to identify a high-resolution product (about 15 km for SNPP/ATMS).

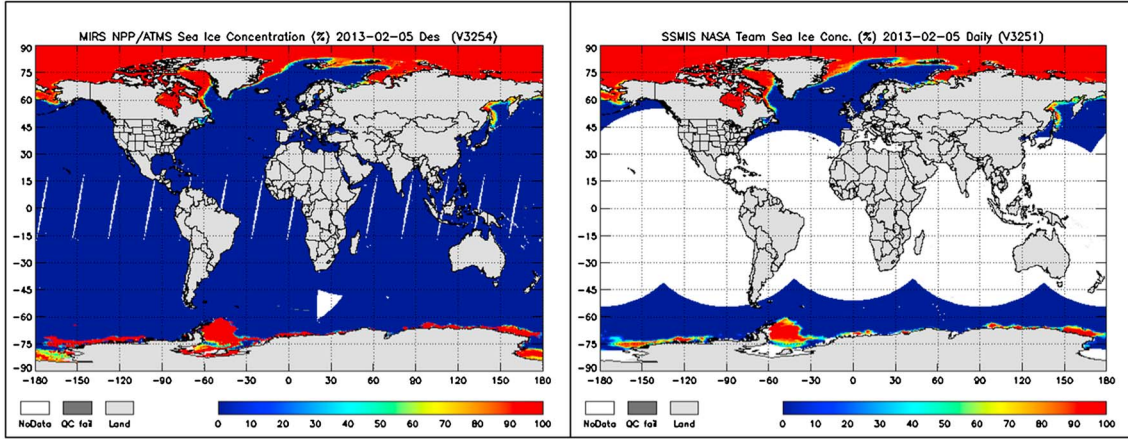


**Figure 19.** Global retrieval of total sea-ice concentration on 5 February 2013 (left) from MiRS SNPP/ATMS and (right) from the near-real-time product from DMSP F17/SSMIS using the NASA Team algorithm.

(MiRS) algorithm to data from the SNPP/ATMS sensor. The products are inverted simultaneously in a land-ocean-atmosphere-cryosphere coupled inversion approach, ensuring that all radiances are fitted simultaneously and ensuring that the geophysical consistency is also satisfied. The assessment of these performances used a mixture of in situ measurements (radiosondes, radar, gauges, and ground-based surface sensors) as well as ECMWF-generated analyses and heritage algorithms. The parameters inverted include the temperature and moisture profiles, the cloud liquid water, ice-water path and rain water path, and the surface rainfall rate. They also include the surface temperature and emissivity as well as the derived snow water equivalent and sea-ice concentration. The assessment focused on those parameters where ground truth exists and is well established and recognized as accurate. We concluded that the temperature and moisture profiles have excellent performances in terms of bias and standard deviation, consistent with and sometimes better than those based on POES and MetOp sensors using the

same algorithm. It is also found that the performances in rainy conditions for temperature sounding are only slightly degraded over ocean but more significantly degraded over land. This is likely due to several factors, but primarily it is believed to be due to the unknown bias correction in those conditions as well as the highly uncertain surface emissivity values. The TPW, which is a simple vertical integration of the moisture profile, is found to be accurate to different degrees across all surfaces including sea ice, snow, land, ocean, and coastal areas. This particular extension of TPW to all surfaces is due to the fact that surface emissivity is included as part of the state vector in the retrieval process. The hydrometeor parameters are difficult to validate. The absence of reliable ground truth and the dependence of the brightness temperatures on parameters that are usually not measured routinely makes this validation challenging. However, given the mechanism employed by MiRS, by which the hydrometeor parameters (CLW, RWP, and IWP) are used to generate a surface rainfall rate based on a

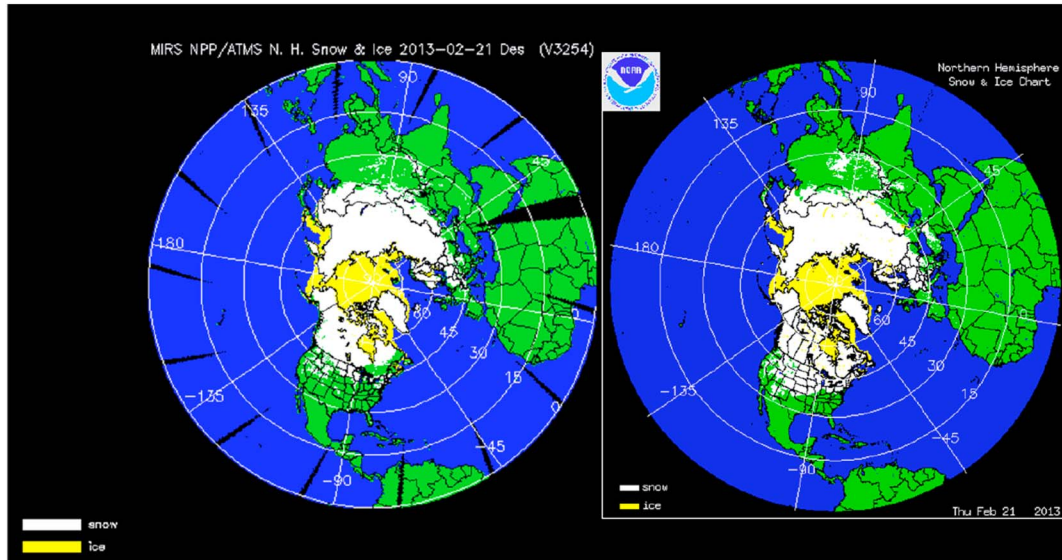


**Figure 20.** Comparison over the Northern Hemisphere of sea-ice extent and snow cover extent on 21 February 2013 from (left) MiRS-ATMS and (right) the National Ice Center IMS operational analysis.

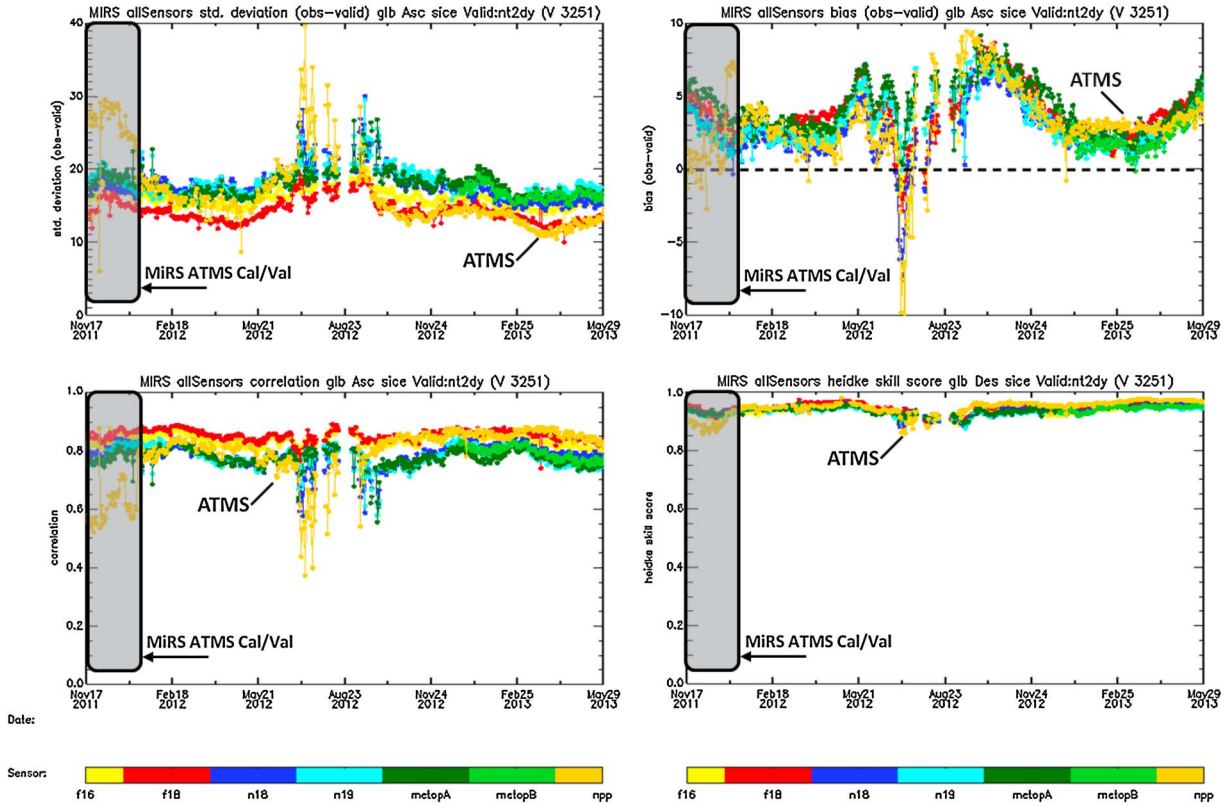


**Figure 21.** Time series of MiRS SIC global performance metrics for seven sensors for the period November 2011 to May 2013. Metrics shown are (top left) difference standard deviation, (top right) bias, (bottom left) correlation, and (bottom right) Heidke Skill Score. MiRS SNPP/ATMS performance is indicated in mustard color. The initial period of calibration and tuning for ATMS and MiRS is shown in gray.

postprocessing relationship developed offline, the validation of the surface rainfall rate (RR) is deemed to be a proxy for the validation of all MiRS-based hydrometeors. The validation of the RR is performed using rain gauges as well as ground-based radars. The performances in terms of RMS, bias, probability of detection, and false alarm were checked independently using the NOAA/NCEP stage IV radar data and the CPC rain gauges analyses. Performances were found to be good and comparable to other sensors. This assessment highlighted the importance of using the proper radiative transfer uncertainty in order to reach the optimal probability of detection and be sensitive to small amounts of rain, while at the same time be mindful not to exacerbate the inevitable false alarm issue.

[35] The surface parameters (land surface temperature and surface emissivities) were extensively validated as well using SURFRAD data, and the performances demonstrated the quality of the SNPP/ATMS products. It is important to note that LST accuracy might not be comparable to IR-based LST inversions but presents the advantage of offering a global, all-weather-conditions coverage. The assessment was stratified by light rain-impacted and nonrainy areas as well as by snow-covered and snow-free surfaces. It is not expected that surface parameters be retrieved with reasonable accuracy under heavy rain conditions where the radiometric signal is saturated. The LST performances reported were also stratified by ground reference sites and were found to depend on the surface characteristics of the area. They have also been assessed against expected simulation-based performances

and deemed reasonable given the many uncertainties in this comparison. More extensive analysis is planned for the LST assessment, including the evaluation of the LST over different seasons, using time series, and the intercomparison with other LST products. Performances of the emissivities at all ATMS channels, including the high frequencies, were assessed against analytically derived emissivities, and the errors were found to be less than 2% when estimates of the errors due to collocation, etc. were accounted for. These emissivities are used as inputs to a postprocessing step that derives cryospheric products (SIC, SCE, and SWE). The SIC was assessed against heritage algorithms (NASA Team algorithm) applied to DMSP F17 SSMIS sensor as well as National Ice Center IMS product. The ice extent is similar to those depicted by IMS, indicating that the polar sounders such as ATMS, AMSU, and SSMIS could be a good complement and/or alternative to the conical microwave imagers such as AMSR, which are traditionally used for cryospheric products generation. This also showed that SNPP/ATMS performances for sea-ice concentration were consistently slightly better than those from other sensors to which MiRS applies (including SSMIS). This is believed due to the higher spatial resolution we run MiRS at for SNPP/ATMS.

[36] Overall, the performances of the SNPP/ATMS derived products, generated using MiRS, are deemed of operational quality and are in the process of being transitioned to operations. The algorithm, which is publicly available, is currently being implemented to run operationally at the NOAA Data Exploitation program.

[37] **Acknowledgments.** The authors would like to acknowledge the CRTM team for their help in getting the CRTM forward operator fine tuned for MiRS applications. The authors would like to thank the main sponsor of the MiRS project, the U.S. NOAA/NESDIS/OSD Product System Development and Implementation (PSDI) program. We also acknowledge A. Reale and the NPROVS team at NESDIS/STAR for providing their matchup data set with global radiosonde used for assessing the MiRS-ATMS sounding products.

## References

- Atkinson, N. (2011), Annex to AAPP scientific documentation: Pre-processing of ATMS and CrIS. Version 1.0. NWP SAF. Doc ID: NWPSAF-MO-UD-027.
- Boukabara, S. A., et al. (2011), MiRS: An all-weather 1DVAR satellite data assimilation and retrieval system, *IEEE Trans. Geosci. Remote Sens.*, **49**(9), 3249–3272, doi:10.1109/tgrs.2011.2158438.
- Boukabara, S. A., K. Garrett, and W. Chen (2010), Global coverage of total precipitable water using a microwave variational algorithm, *IEEE Trans. Geosci. Remote Sens.*, **48**(10), 3608–3621, doi:10.1109/tgrs.2010.2048035.
- Chen, M., W. Shi, P. Xie, V. B. S. Silva, V. E. Kousky, R. W. Higgins, and J. E. Janowiak (2008), Assessing objective techniques for gauge-based analyses of global daily precipitation, *J. Geophys. Res.*, **113**, D04110, doi:10.1029/2007JD009132.
- Ferraro, R., et al. (2013), An evaluation of microwave land surface emissivities over the continental United States to benefit GPM-Era precipitation algorithms, *IEEE Trans. Geosci. Remote Sens.*, **51**(1), 378–398, doi:10.1109/tgrs.2012.2199121.
- Holmes, T. R. H., R. A. M. De Jeu, M. Owe, and A. J. Dolman (2009), Land surface temperature from Ka band (37 GHz) passive microwave observations, *J. Geophys. Res.*, **114**, D04113, doi:10.1029/2008JD010257.
- Iturbide-Sanchez, F., S. A. Boukabara, R. Y. Chen, K. Garrett, C. Grassotti, W. Chen, and F. Weng (2011), Assessment of a variational inversion system for rainfall rate over land and water surfaces, *IEEE Trans. Geosci. Remote Sens.*, **49**(9), 3311–3333, doi:10.1109/tgrs.2011.2119375.
- Kongoli, C., et al. (2011), A new sea-ice concentration algorithm based on microwave surface emissivities—Application to AMSU measurements, *IEEE Trans. Geosci. Remote Sens.*, **49**(1), 175–189, doi:10.1109/tgrs.2010.2052812Y.
- Lin, Y., and K. E. Mitchell (2005), The NCEP stage II/IV hourly precipitation analyses: Development and applications, presented at the Proc. 19<sup>th</sup> Conf. Hydrol., Amer. Meteorol. Soc., San Diego, CA, Paper 1.2.
- Liu, Q., F. Weng, and S. English (2011), An improved fast microwave water emissivity model, *IEEE Trans. Geosci. Remote Sens.*, **49**, 1238–1250.
- Liu, Q., P. van Delst, Y. Chen, D. Groff, Y. Han, A. Collard, F. Weng, S. A. Boukabara, and J. Derber (2012), Community Radiative Transfer Model for Radiance Assimilation and Applications, IEEE International Geoscience and Remote Sensing Symposium (IGARSS) proceedings, Pages: 3700–3703.
- Long, D., and D. Daum (1998), Spatial resolution enhancement of SSM/I data, *IEEE Trans. Geosci. Remote Sens.*, **36**(2), 407–417.
- Norouzi, H., W. Rossow, M. Temimi, C. Prigent, M. Azarderakhsh, S. A. Boukabara, and R. Khanbilvardi (2012), Using microwave brightness temperature diurnal cycle to improve emissivity retrievals over land, *Remote Sens. Environ.*, **123**, 470–482, doi:10.1016/j.rse.2012.04.015.
- Parinussa, R. M., R. A. M. De Jeu, T. R. H. Holmes, and J. P. Walker (2008), Comparison of microwave and infrared land surface temperature products over the NAFE'06 research sites, *IEEE Geosci. Remote Sens. Lett.*, **5**(4), 783–787.
- Prigent, C., E. Jaumouille, F. Chevallier, and F. Aires (2008), A parameterization of the microwave land surface emissivity between 19 and 100 GHz, anchored to satellite-derived estimates, *IEEE Trans. Geosci. Remote Sens.*, **46**, 344–352.
- Reale, A., B. Sun, F. Tilley, and M. Petter (2012), NOAA Products Validation System (NPROVS), *J. Atmos. Oceanic Technol.*, **29**, 629–645.
- Weng, F., B. Yan, and N. C. Grody (2001), A microwave land emissivity model, *J. Geophys. Res.*, **106**(D17), 20,115–20,123, doi:10.1029/2001JD900019.
- Yu, Y., D. Tarpley, J. Privette, M. Goldberg, M. Raja, K. Vinnikov, and H. Xu (2009), Developing algorithm for operational GOES-R land surface, temperature product, *IEEE Trans. Geosci. Remote Sens.*, **47**(3), 936–951.
- Zou, X., L. Lin, and F. Weng (2013), Absolute calibration of ATMS upper level temperature sounding channels using GPS RO observations, *IEEE Trans. Geosci. Remote Sens.*, **PP**(99), 1, doi:10.1109/tgrs.2013.2250981.